SAND80-2646
Unlimited Release
UC-60

Vertical Axis Wind Turbine Drive Train Transient Dynamics

David B. Clauss, Thomas G. Carne

Sandia National Laboratories

SF 2900-Q(3-80)

Issued by Sandia National Laboratories, operated for the United States Department of Energy by Sandia Corporation.

Printed in the United States of America

Available from:

National Technical Information Service
U. S. Department of Commerce
5285 Port Royal Road
Springfield, VA 22161

NTIS Price Codes:

Printed Copy $7.00; Microfiche: A04

SAND80-2646

Vertical Axis Wind Turbine Drive Train Transient Dynamics*

David B. Clauss
Thomas G. Carne
Division 5523
Sandia National Laboratories**
Albuquerque, New Mexico 87185

Abstract

Start-up of a vertical axis wind turbine causes transient torque oscillations in the drive train with peak torques which may be over two and one-half times the rated torque of the turbine. These peak torques are of sufficient magnitude to possibly damage the drive train; safe and reliable operation requires that mechanical components be overdesigned to carry the peak torques caused by transient events. A computer code, based on a lumped parameter model of the drive train, has been developed and tested for the Low Cost 17-Meter turbine; the results show excellent agreement with field data. The code has subsequently been used to predict the effect of a slip clutch on transient torque oscillations. It has been demonstrated that a slip clutch located between the motor and brake can reduce peak torques by thirty eight percent.

* This work was supported by the U.S. Department of Energy Contract DE-AC094-76DP00789

** A. U.S. Department of Energy Facility

Contents

Illustrations

Introduction

Transient events during operation of Darrieus vertical-axis wind turbines can cause torque levels in the drive line which are unacceptable for many components. Start-up and braking in various ambient conditions are typical events during which peak torques may reach excessive magnitudes. Experience with research vertical axis wind turbines (VAWT) indicates that peak torques of 2 to 3 times rated torque are typical during starting and braking, which implies an undesired overdesign of drive-line components. The objective of the present investigation is to develop an analytical tool which can be used to predict drive-train behavior for several different loading conditions.

Analysis is needed to determine which starting and braking methods are most effective in reducing the peak torques seen in the drive-line. Areas deserving investigation include start-up in high winds, as well as electrical and mechanical methods (clutches) designed to achieve a softer start. The relative effectiveness of low speed vs. high speed braking, and definition of a braking rate which will decrease dynamic amplification to an acceptable level also merit study. Although this paper will deal primarily with turbine start-up in zero ambient wind speed and the effects of a slip clutch on transient response, the model can easily be adapted to study the problems mentioned above.

The model and the numerical results as well are based on experimental data obtained on the Low Cost 17M VAWT installed at Rocky Flats, CO, Figure 1. The method, however, is essentially general to all VAWT's. A Fortran program called DYDTA (DYnamic Drive Train Analysis) numerically evaluates the differential equations of motion and plots results. The program is briefly described in Appendix A.

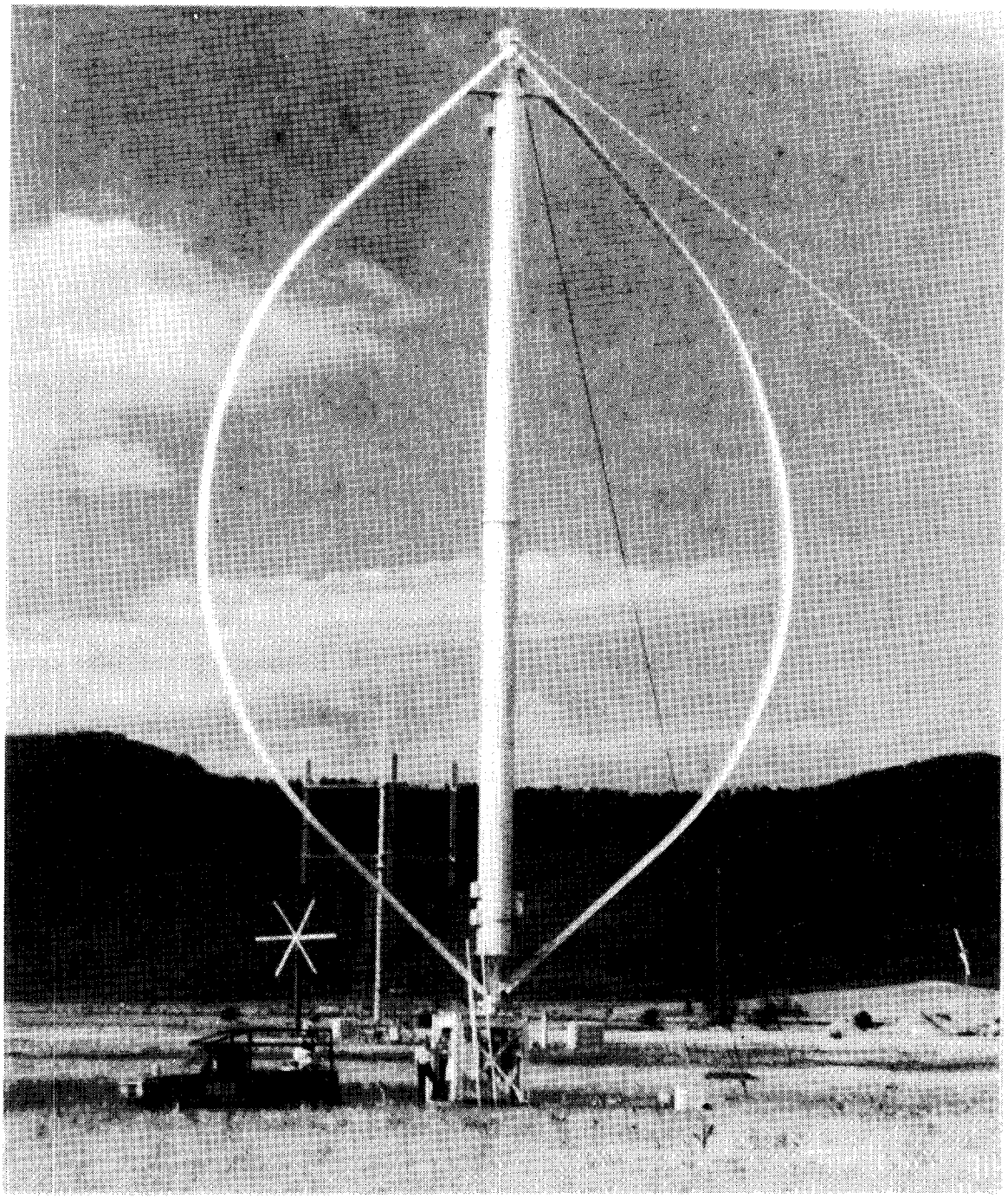

Figure 1. DOE/ALCOA Low Cost 17M Vertical Axis Wind Turbine installed at Rocky Flats, CO.

The Drive Train Model

Typically, a VAWT drive train consists of the turbine rotor (blades and rotating tower), the transmission, a brake disc and an induction motor/generator which are connected in series by shafts and couplings. Additional mechanical components may be present, and the drive train topography may vary depending upon the specific turbine design. Additional components may include a timing belt (for incremental adjustment of turbine operating speed) and/or a slip clutch. The position of the brake relative to the transmission and clutch, if present, is the most variable element in drive train topography. For instance on the Low Cost 17M turbine at Rocky Flats, Figure 1, the brake is on the high speed shaft, whereas earlier turbines have had the brake on the low speed shaft.

The transient response depends on the natural characteristics of the system and the functional form of the applied torques. The physical representation of the drive train is shown in Figure 2, along with physical values for the Low Cost turbine. For generality the model includes the slip clutch, as well as applied torques on each inertial element. Several assumptions are made, all of which may not be applicable to a given VAWT design. The low speed shaft is considered to be the only significant stiffness in the system since, in an equivalent system, it appears much softer than both the high speed shaft and the rotating tower. As larger turbines are built and tower height increases, the tower stiffness may approach the same value of stiffness as the low speed shaft, and at some point tower stiffness may have to be included in the model. On the other hand, the effect of the transmission's gear ratio on the equivalent stiffness of the high speed shaft seems to insure that the high speed stiffness will remain large relative to low speed stiffness, and thus the high speed shaft can be effectively modeled as a rigid element. The motor torque curve as specified by the manufacturer is modified by a constant scale factor less than

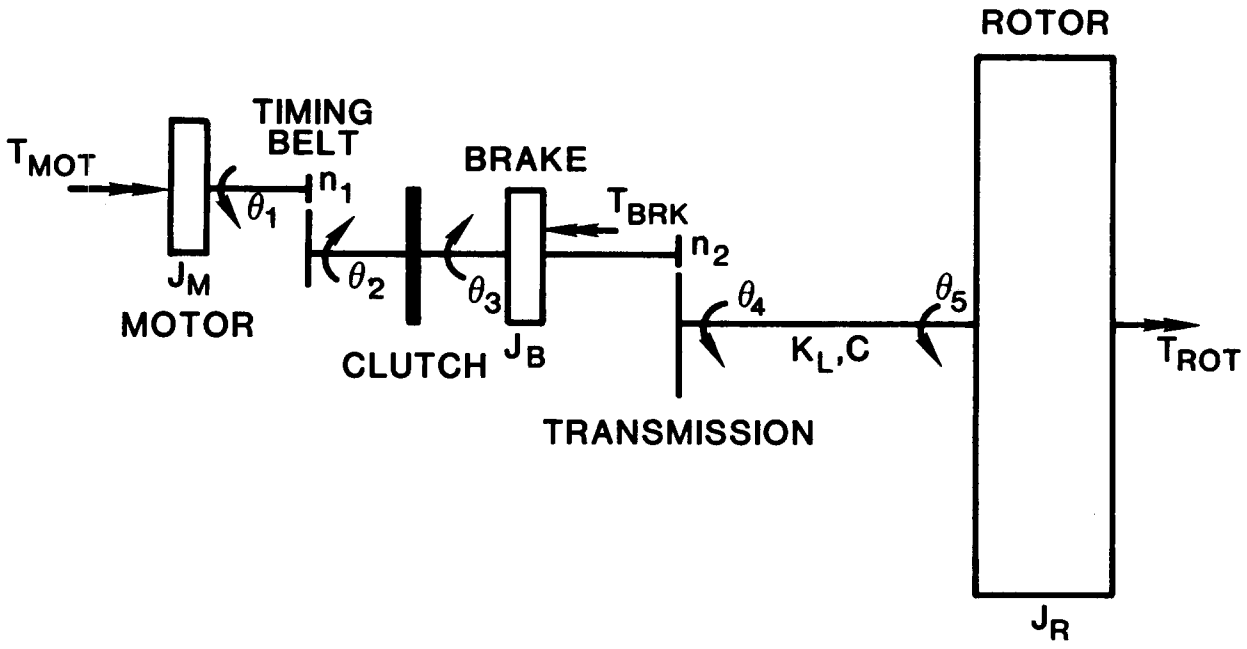

J_M = motor inertia = 1.291 lb-ft-s^2

J_B = brake inertia = 1.598 lb-ft-s^2

J_R = rotor inertia = 4.042 x 10^4 lb-ft-s^2

C = Viscous damping = 1.1 x 10^3 lb-ft-s

K_L = low speed shaft stiffness = 8.626 x 10^5 lb-ft

n_1 = timing belt ratio = 1, 40/38, 44/38

n_2 = transmission ratio = 35.07

T_{MOT} = motor torque, $T_{MOT}(\omega)$

T_{BRK} = brake torque, $T_{BRK}(t)$

T_{ROT} = aerodynamic torque, $T_{ROT}(\omega, t)$

Figure 2. Physical Representation of VAWT Drive Train.

one, which is related to the voltage drop in the line. For an induction motor/generator, torque is proportional to voltage squared, so that a 20% drop in voltage will cause a 36% reduction in motor torque. The assumption of a constant motor scale factor implies that the voltage drop, and thus the current drawn by the motor are independent of motor speed, which is only approximately true. Also, nonlinear effects such as Coulomb friction, aerodynamic damping, and drive slack are not treated. All losses are represented by viscous damping.

The equations of motions describing the torsional response of the drive train can be easily written by drawing free body diagrams for each inertial element, Figure 3, and equating the torque on each to zero. This method is preferred because it

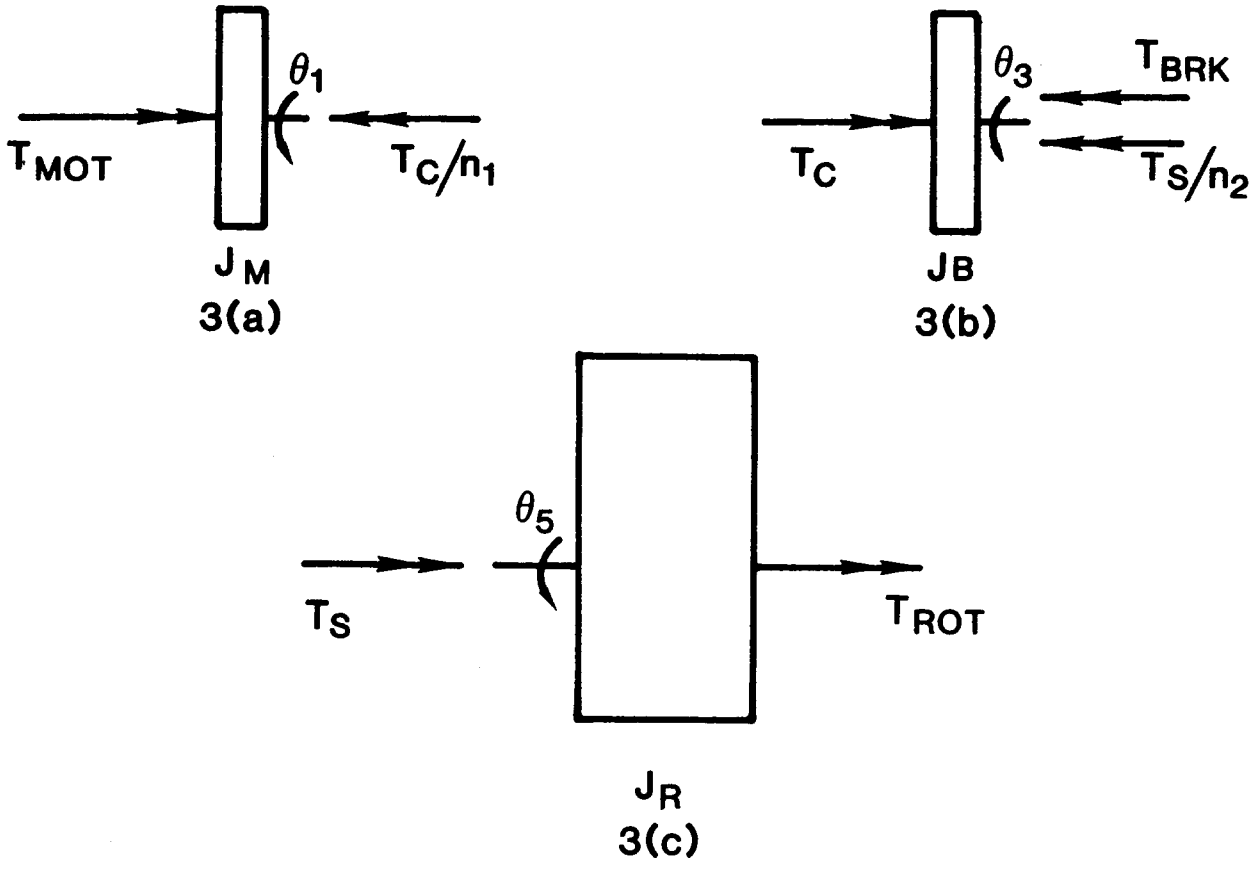

Figure 3. Free Body Diagrams for writing equations of motion.

permits treatment of the nonlinear effect of the clutch in a simple way since torque through the clutch can be expressed explicitly. Referring to Figures 2 and 3, T_c and T_s are defined and calculated as follows:

T_s = torque transmitted through low speed shaft,

$$T_s = K_L(\theta_4 - \theta_5) + C(\dot{\theta}_4 - \dot{\theta}_5), \tag{1}$$

T_c = torque transmitted through slip clutch.

The equations of motion can now be written directly:

$$J_M\ddot{\theta}_1 = T_{MOT} - T_c/n_1, \tag{2}$$

$$J_B\ddot{\theta}_3 = T_c - T_{BRK} - T_s/n_2, \tag{3}$$

$$J_R\ddot{\theta}_5 = T_s + T_{ROT}, \tag{4}$$

where the clutch imposes a constraint of the form

$$|T_c| \leq T_{max}; \tag{5}$$

T_{max} = maximum torque passed by clutch.

The slip clutch typically consists of two mating frictional surfaces which are connected to the driving and driven shafts, respectively. These frictional surfaces are compressed together by a spring, so that the normal force, surface area, and friction coefficients determine the maximum torque transmitted by the clutch. T_{max} can be adjusted by changing the spring deflection.

The clutch is always operating in one of two conditions; it is either engaged, in which case the velocities on either side of the clutch are equal, or it is slipping, in which case the velocities are unequal and the clutch torque is equal to $\pm T_{max}$. The torque speed characteristic of an ideal clutch is shown in Figure 4. Note that T_{max} is a restoring torque; that is, it is in a direction that will tend to re-engage the clutch.

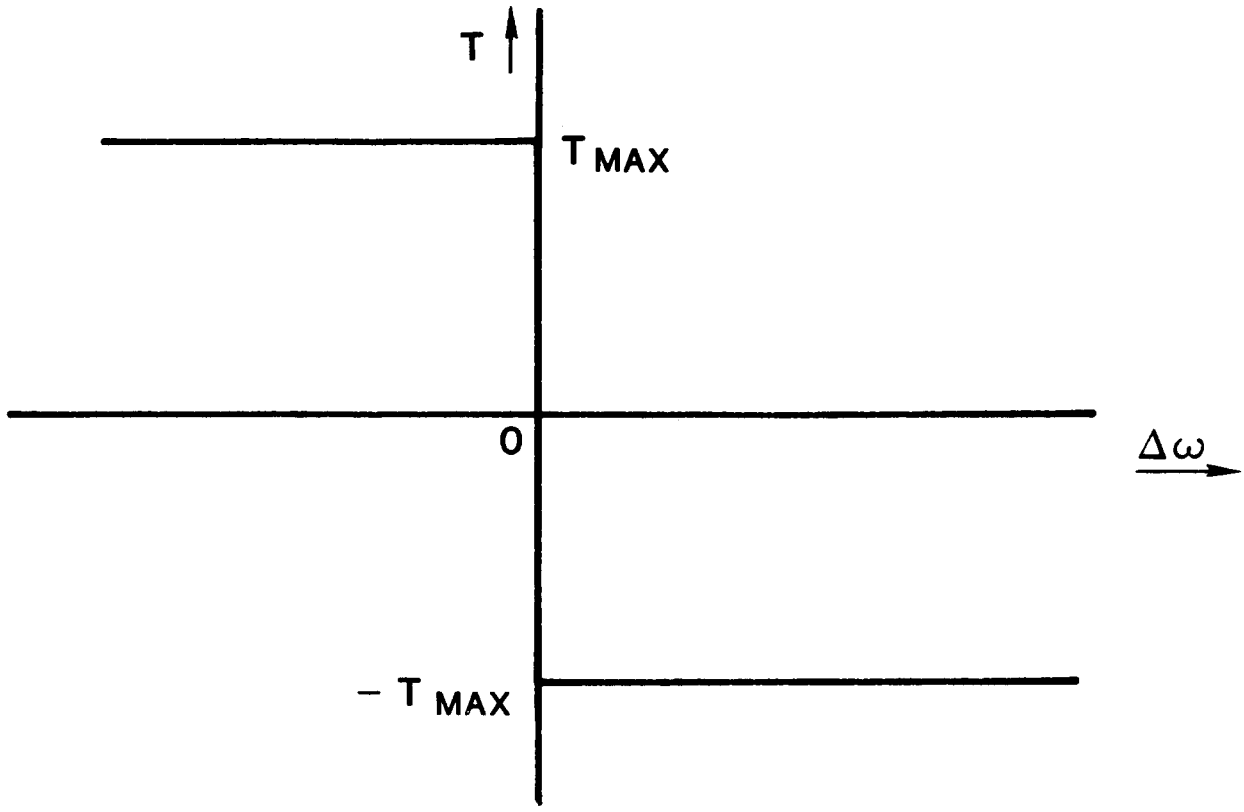

Figure 4. Torque vs. Speed Difference - Ideal Clutch. Assumes static friction coefficient equals dynamic friction coefficient.

With this understanding, two distinct sets of unconstrained equations of motion can be written corresponding to the two operating states of the clutch, which will be referred to as the engagement and slip equations, respectively.

Engagement of the slip clutch implies that $\dot{\theta}_2 = \dot{\theta}_3$, so that the motor and brake move together. Multiplying equation (2) by n_1 and summing the result with equation (3):

$$n_1 J_M \ddot{\theta}_1 + J_B \ddot{\theta}_3 = n_1 T_{MOT} - T_{BRK} - T_s/n_2 \ . \qquad (6)$$

The equations can be simplified by making the following variable transformation and taking advantage of gear relations

$$\psi_1 = \theta_2 = \theta_1/n_1, \tag{7}$$

$$\psi_2 = \theta_3 = n_2\theta_4, \tag{8}$$

$$\psi_3 = n_2\theta_5. \tag{9}$$

Thus the complete set of engagement equations can be written

$$(J_{ME} + J_B)\ddot{\psi}_1 = n_1 T_{MOT} - T_{BRK} - K_{LE}(\psi_2-\psi_3) - C_E(\dot{\psi}_2-\dot{\psi}_3), \tag{10}$$

$$\ddot{\psi}_2 = \ddot{\psi}_1, \tag{11}$$

$$J_{RE}\ddot{\psi}_3 = K_{LE}(\psi_2-\psi_3) + C_E(\dot{\psi}_2-\dot{\psi}_3) + T_{ROT}/n_2; \tag{12}$$

where

$$J_{ME} = n_1^2 J_M, \tag{13}$$

$$J_{RE} = J_R/n_2^2, \tag{14}$$

$$K_{LE} = K_L/n_2^2, \tag{15}$$

$$C_E = C/n_2^2. \tag{16}$$

Slipping of the clutch decouples the motor from the brake and rotor, so that the slip equations describe two independent systems as shown in Figure 5. Slip implies a velocity difference across the clutch and that the torque transmitted through the clutch is a constant $\pm T_{max}$. Again taking advantage of equations (7) - (9) and equations (13) - (16), and making the substitution

$$T_C = \pm T_{max} \tag{17}$$

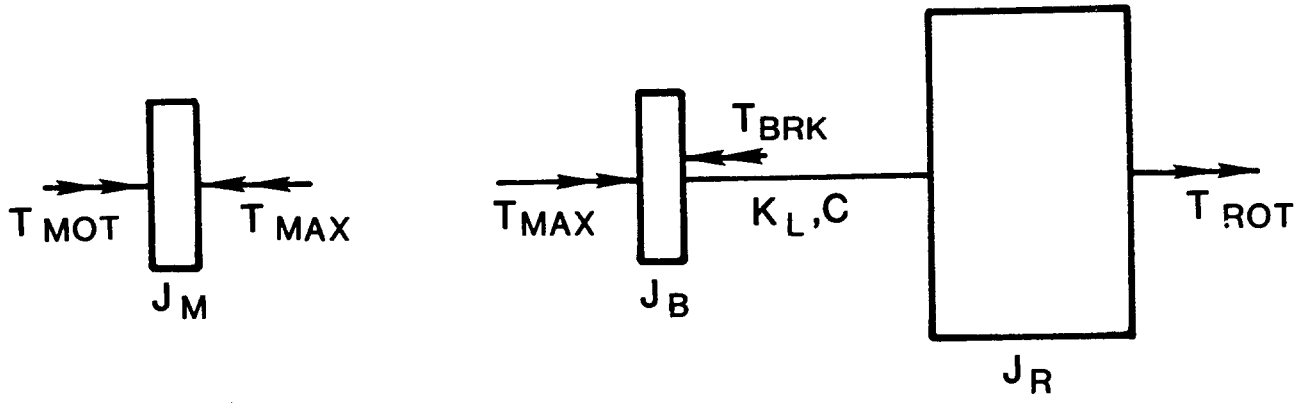

5(a) - motor system

5(b) - brake rotor system

Figure 5. Representation of Drive Train for clutch slipping.

the final form of the slip equations becomes

$$J_{ME}\ddot{\psi}_1 = n_1 T_{MOT} \mp T_{max}, \tag{18}$$

$$J_B\ddot{\psi}_2 = \pm T_{max} - T_{BRK} - K_{LE}(\psi_2 - \psi_3) - Ce(\dot{\psi}_2 - \dot{\psi}_3), \tag{19}$$

$$J_{RE}\ddot{\psi}_3 = K_{LE}(\psi_2 - \psi_3) + C_E(\dot{\psi}_2 - \dot{\psi}_3) + T_{ROT}/n_2, \tag{20}$$

where T_{max} is positive for motor overspeed.

The conditions for initiation of slip and for re-engagement are somewhat more subtle, although intuitively simple. Assume that, at time equal zero, the clutch is engaged. Slip initiates when the clutch torque equals T_{max} and continued engagement would tend to violate the constraint, equation (5). Stated more rigorously the initiation of slip occurs when

$$T_{Ce} = T_{max} \tag{21}$$

and

$$\frac{dT_{Ce}}{dt} > 0 \tag{22}$$

where the subscript e indicates the result obtained from the engagement equations. If T_{Ce} is negative, then inequality (22) is directed in the opposite sense. Now assume that the clutch is slipping, so that $\dot{\theta}_2 \neq \dot{\theta}_3$. Re-engagement occurs when the velocities across the clutch become equal again:

$$\dot{\theta}_{2s} = \dot{\theta}_{3s} \tag{23}$$

and if

$$|T_{Ce}| \leq T_{max}.$$

At re-engagement there must be a discontinuity in acceleration, which implies a discontinuity in the clutch torque. This is consistent with the characteristics of the clutch as shown in Figure 4, since when $\Delta\omega = 0$ (as it is at re-engagement), the clutch torque may be any value between positive T_{max} and negative T_{max}. A more complete description of the behavior of a slip clutch is given in Appendix B, with the consequences of the clutch illustrated.

Thus, a basic algorithm would be to use the engagement equations until equations (21) and (22) are satisfied (slip initiates), and then to apply the slip equations until equation (23) is met (re-engagement), at which point the algorithm is applied recursively.

A great deal of insight can be gained from an examination of the natural characteristics of the system, especially in the case of start-up. The remainder of this paper will focus on start-up in a zero ambient wind speed. The motor torque-speed characteristic has a significant impact on the natural characteristics of the system. A typical induction motor curve is shown in Figure 6. It is important to realize

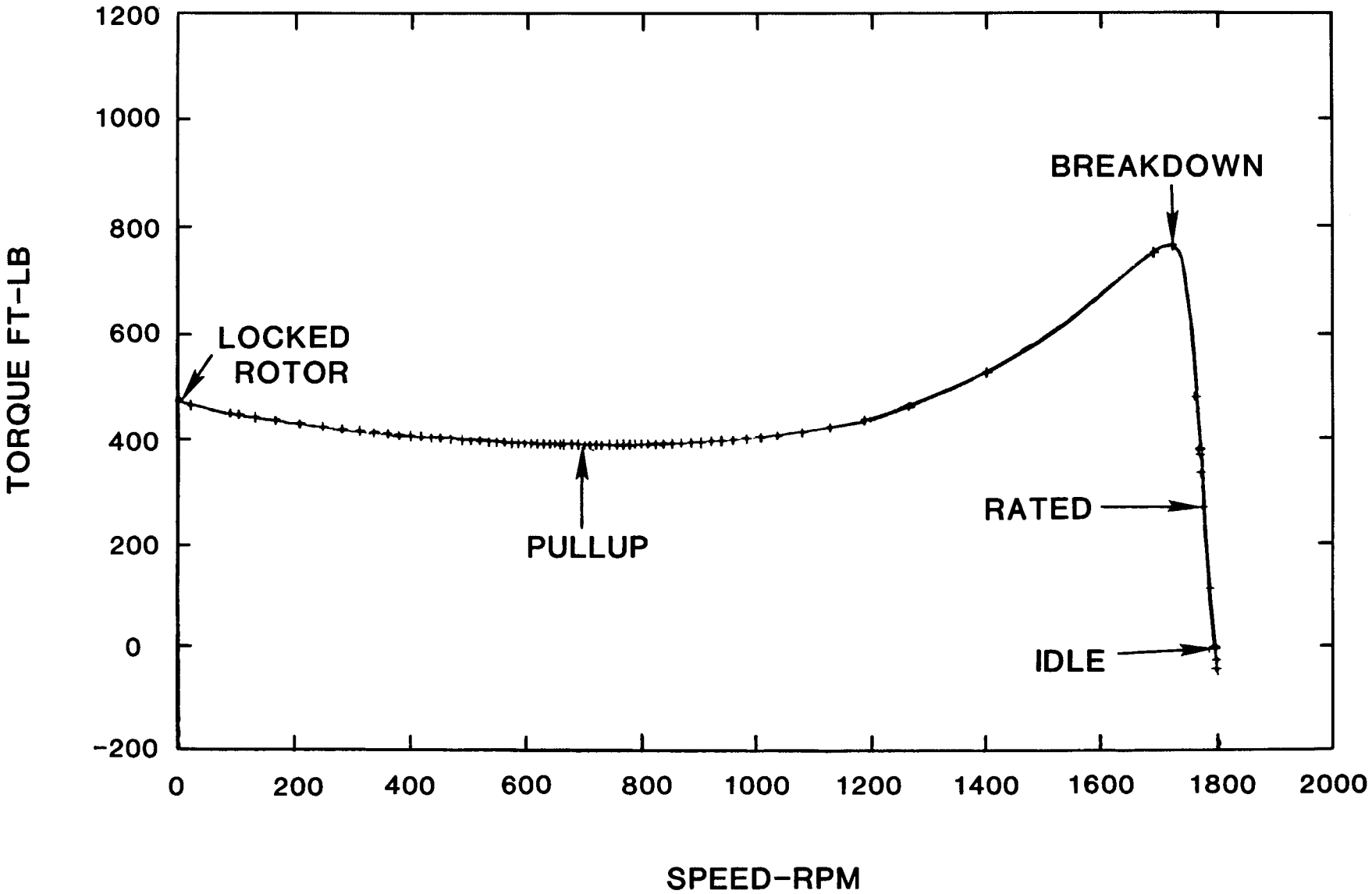

Figure 6. Torque-Speed characteristic of an induction motor.

that motor torque is a function of motor speed, not of time. Torque ripple models developed[1] by Reuter have treated the induction motor/generator mechanically as an inertia connected to ground through a linear viscous damper. Referring to Figure 6 the torque-speed relationship is indeed linear for steady state operation ($1740 < \omega < 1860$ rpm). However, during start-up the motor speed goes from 0 to 1800 rpm and the torque-speed relationship cannot be represented as a linear element. From an intuitive standpoint, it is most clear to think of the motor torque characteristic as a non-linear damper, which has a coefficient dependent on rpm, superimposed on a step torque, though in the code and model it is treated as an applied torque. To be clear, the motor torque should not be considered to be an external torque because it is not independent of the state of the system. With this in mind, the free vibration characteristics of the drive train during start-up can be considered.

The natural characteristics of the system also depend on the operating state of the slip clutch. When the clutch is engaged, there is an effectively rigid connection between the motor and the brake so their respective inertias may be lumped together, and the system can be represented as shown in Figure 7. On the other hand, slipping decouples the motor and creates two independent systems, Figure 8. The latter case will not be treated in detail, however, it is apparent that the fundamental frequency of the decoupled system in 8(b) will be higher than that of coupled system in Figure (7), and that the isolated motor, Figure 8(a) moves as a rigid body.

Due to the nonlinearity introduced into the system by the motor and clutch, a linear eigenvalue analysis is not truly applicable. The equivalent motor damping changes continually so that the natural frequencies and mode shapes are a function of speed. However, an approximate analysis can be done by considering two subcases based on motor speed less than or

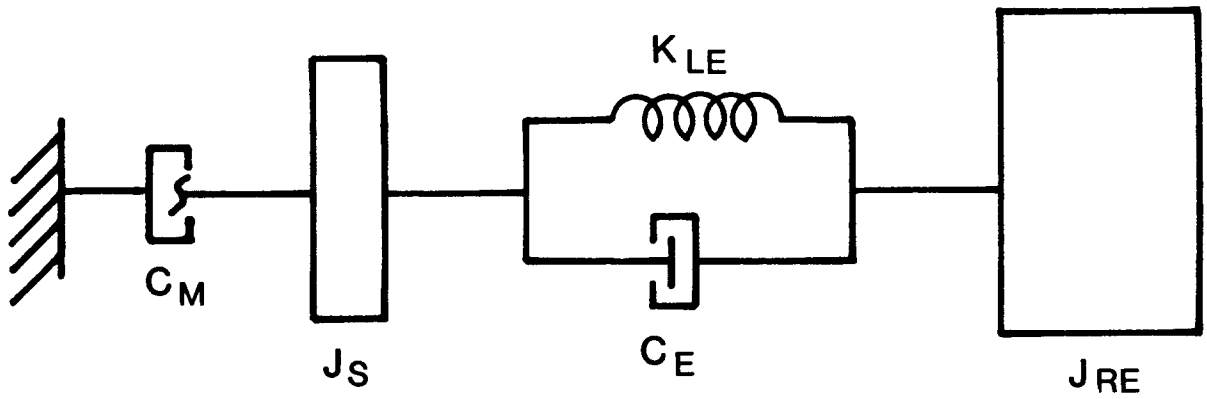

$$J_S = n_1^2 \; J_M + J_B$$

Figure 7. System representation with clutch engaged.

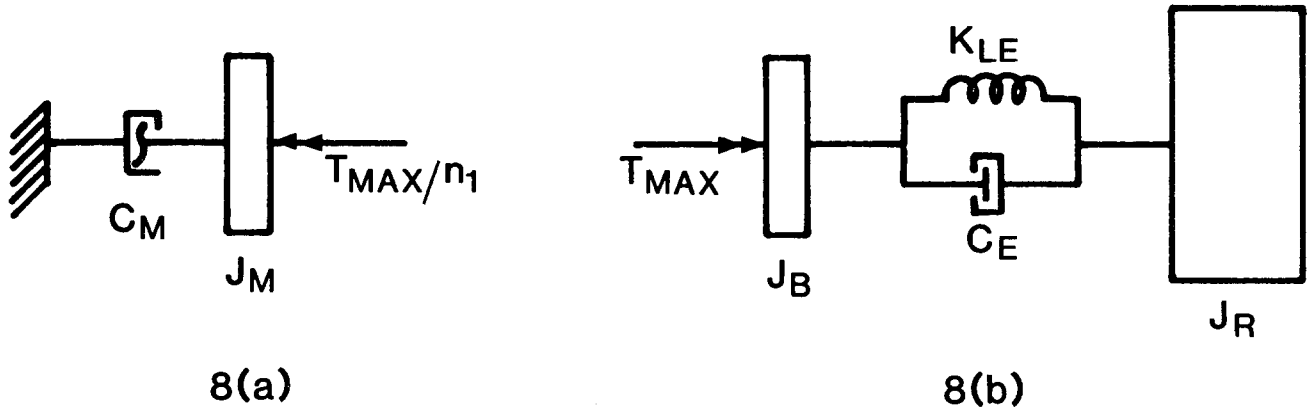

Figure 8. System representation with clutch slipping.

greater than the motor breakdown speed, respectively. Up to the breakdown speed the maximum absolute instantaneous motor damping results in a critical damping of approximately minus nine percent, and consequently the damping does not greatly affect the natural frequencies up to breakdown speed. Note that negative damping has the same effect on frequency as

positive damping (1 d.o.f., $\omega_d = \sqrt{1 - \zeta^2}\,\omega_n$), but the opposite effect on mode shape (in Figure 7, negative damping from the motor tends to increase the oscillations of the motor and brake relative to the rotor). Thus, up to breakdown, damping is negligible and the system can be viewed as shown in Figure 9(a). The natural frequencies and mode shapes of the

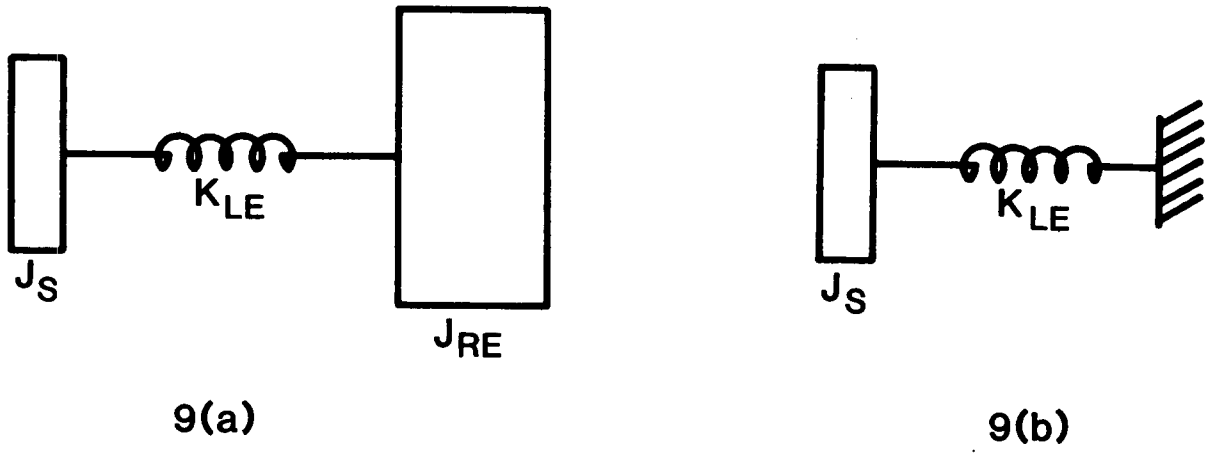

Figure 9. System representation with clutch engaged and motor speed < 1720 rpm.

system in Figure 9(a) are easily determined. The results are

$$\omega = 0,\ \sqrt{\frac{K_{LE}(J_S + J_{RE})}{J_S J_{RE}}} \tag{24}$$

$$= 0,\quad 2.586\quad \text{HZ}$$

$$u^{(1)} = \begin{Bmatrix} 1.000 \\ 1.000 \end{Bmatrix},\quad u^{(2)} = \begin{Bmatrix} 1.000 \\ 1 - \dfrac{J_S + J_{RE}}{J_{RE}} \end{Bmatrix} \tag{25}$$

$$= \begin{Bmatrix} 1.000 \\ -0.083 \end{Bmatrix}$$

The mode shape indicates that the generator/brake is moving with much greater amplitude than the rotor, so that the mode basically represents the motor/brake winding up about the low speed shaft, Figure 9(b). Indeed, if $J_{RE} >> J_S$ (typically the case for VAWT's), equation (24) can be approximated by

$$\omega \simeq \sqrt{\frac{K_{LE}}{J_S}} \tag{26}$$

which corresponds to the frequency of the system in Figure 9(b).

As previously discussed, when the motor speed is greater than the breakdown speed, the torque is nearly a linear function of speed, with a very large negative slope. This slope, and thus the effective damping, is a function of the rated power, the synchronous speed, and the slip at rating for an induction motor/generator:

$$C_M = \frac{P_{rated}}{\Omega^2 S} \quad , \tag{27}$$

as given in [2].

For the Low Cost turbine this corresponds to a critical damping factor of over 200%, which indicates that the generator/brake oscillation will be very small. As an approximation, the generator can then be considered to be fixed when the motor speed is greater than the breakdown speed, as shown in Figure 10, so that the first mode resembles the rotor winding up on the low speed shaft.

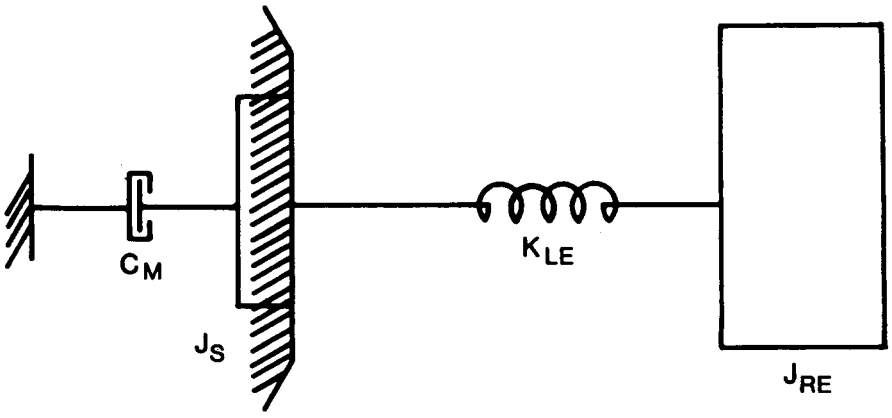

Figure 10. System representation with clutch engaged and motor speed > 1730 rpm.

The frequency for the system in Figure 10 is simply

$$\omega \cong \sqrt{\frac{K_{LE}}{J_{RE}}} \quad . \tag{28}$$

Experimental Record - Base Case

The Low Cost 17M turbine at Rocky Flats is instrumented with a torque sensor located on the low speed shaft. A typical start-up record taken in zero ambient wind speed is shown in Figure 11. The experimental record was used to develop a base case which could be used to verify the predictive capabilities of the model, as well as to fix certain parameters that could not accurately be calculated analytically or experimentally. The parameters which were varied were the viscous damping coefficient and the motor scale factor. There are several characteristics which are typical of a start-up record: the initial overshoot and subsequent decay, and then the growth of torque oscillations to the largest peak torque, and the frequency shift that occurs just after the peak is reached. Note that the maximum torque (40,000 ft-lb) is over 2.5 times the rated turbine torque (15,000 ft-lb). The time to start is also an important characteristic. Several non-linear effects are apparent in the record as well; the decay envelope is not smooth, which indicates non-viscous damping, and gear slack is evident (note the 'notch' when the sign of the torque changes near the end of the record). The model does not attempt to explain or predict these non-linear effects.

DYDTA results for this base case are shown in Figures 12-15. Varying the motor scale factor changes the starting time and the magnitude of torque, while varying the viscous damping coefficient primarily affects the initial rate of decay and to a lesser extent the magnitude of torque oscillations. The final value for the motor scale factor is 0.665, which

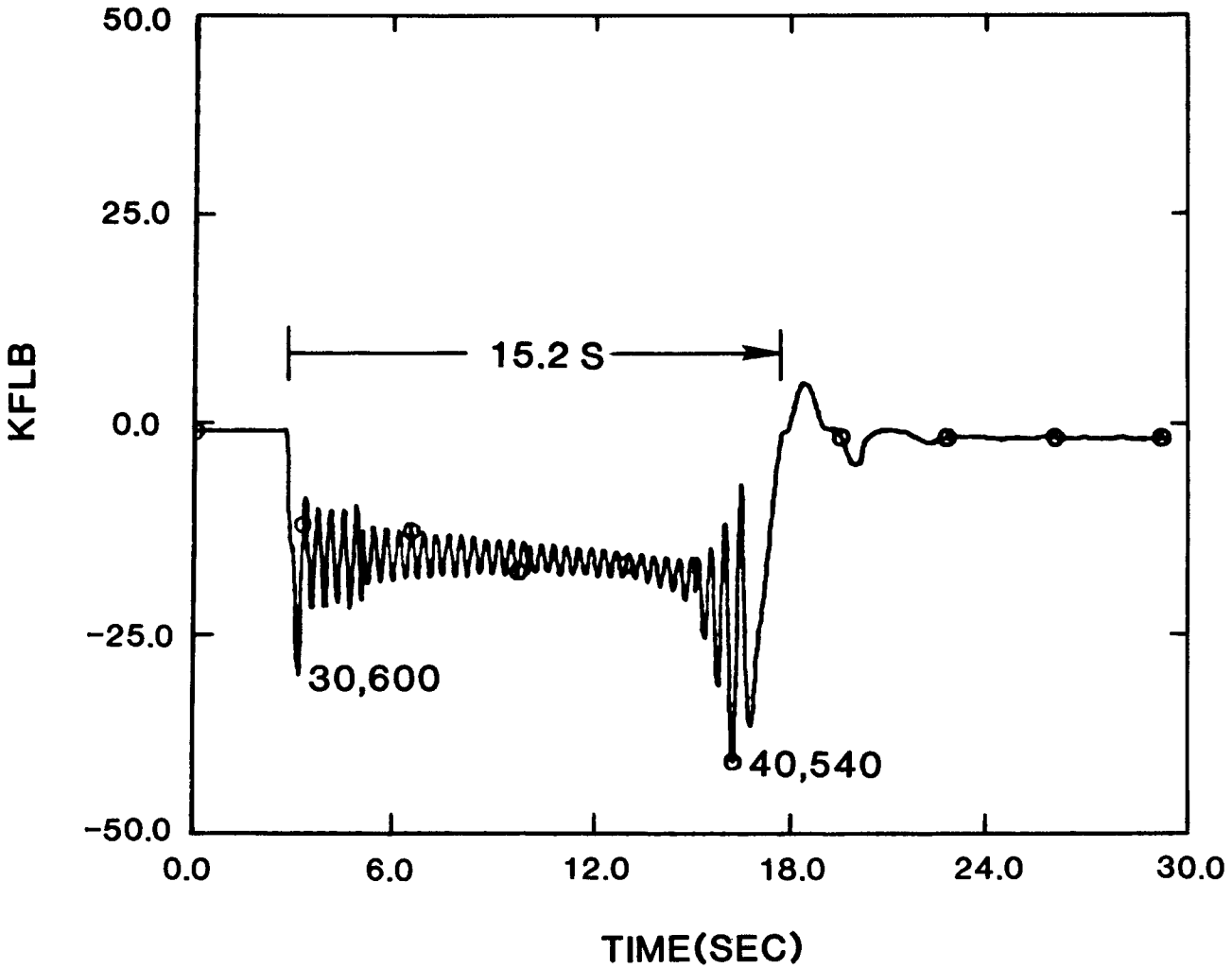

Figure 11. Experimental Record - Low speed shaft torque vs. time for the Low Cost turbine start-up in zero wind.

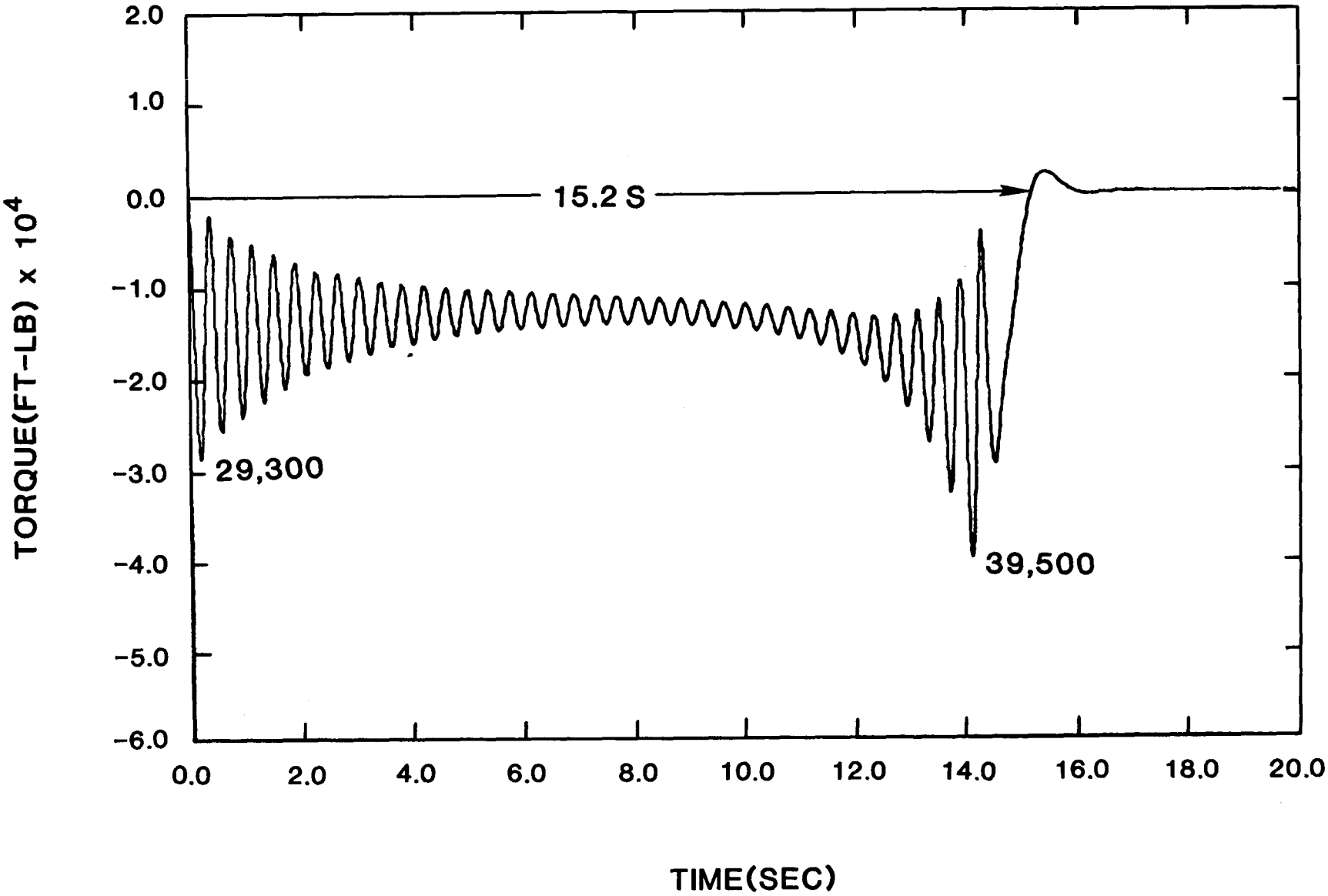

Figure 12. DYDTA prediction - Low speed shaft torque vs. time during start-up in zero wind - no clutch.

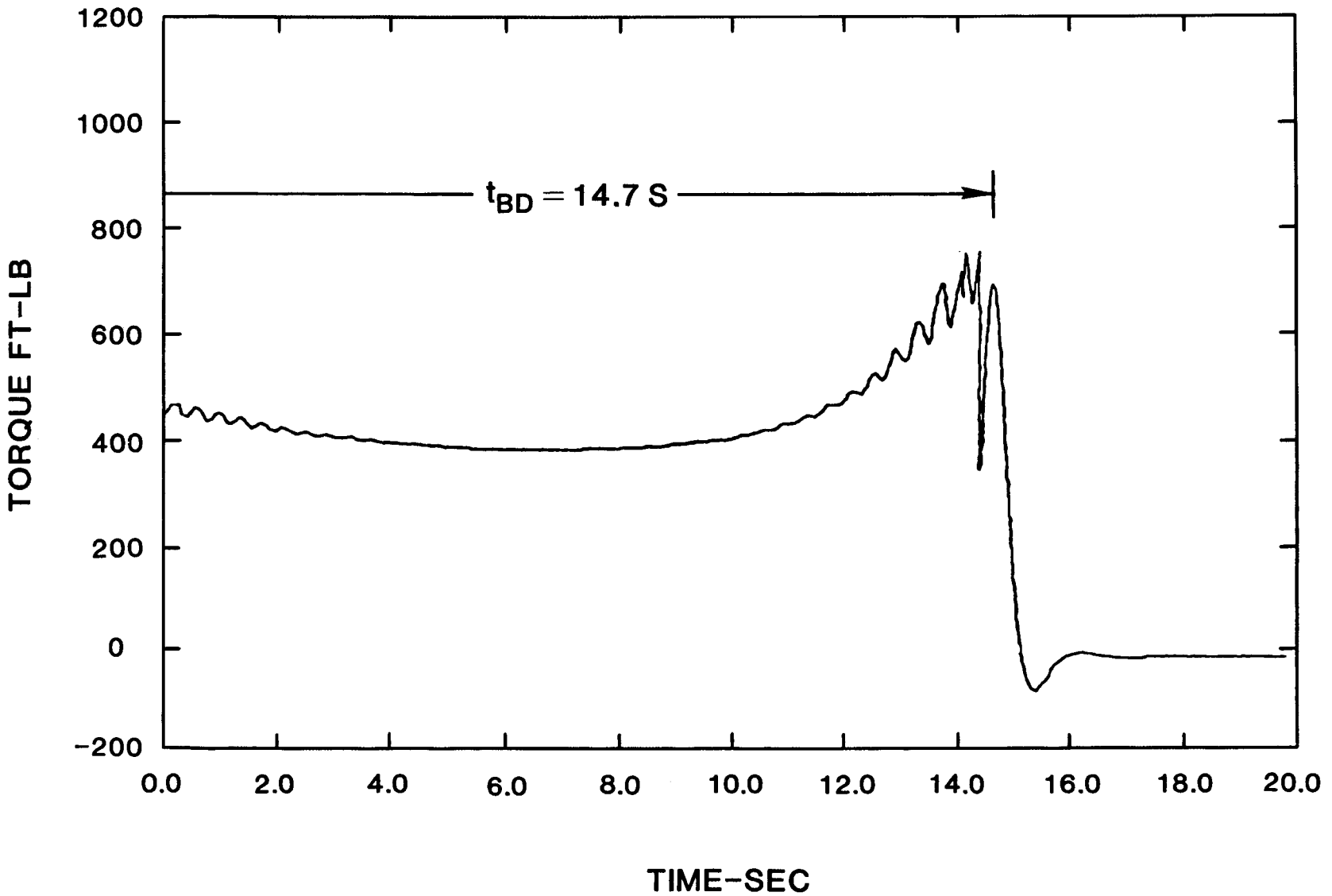

Figure 13. DYDTA prediction - Motor torque vs. time for start-up in zero wind - no clutch.

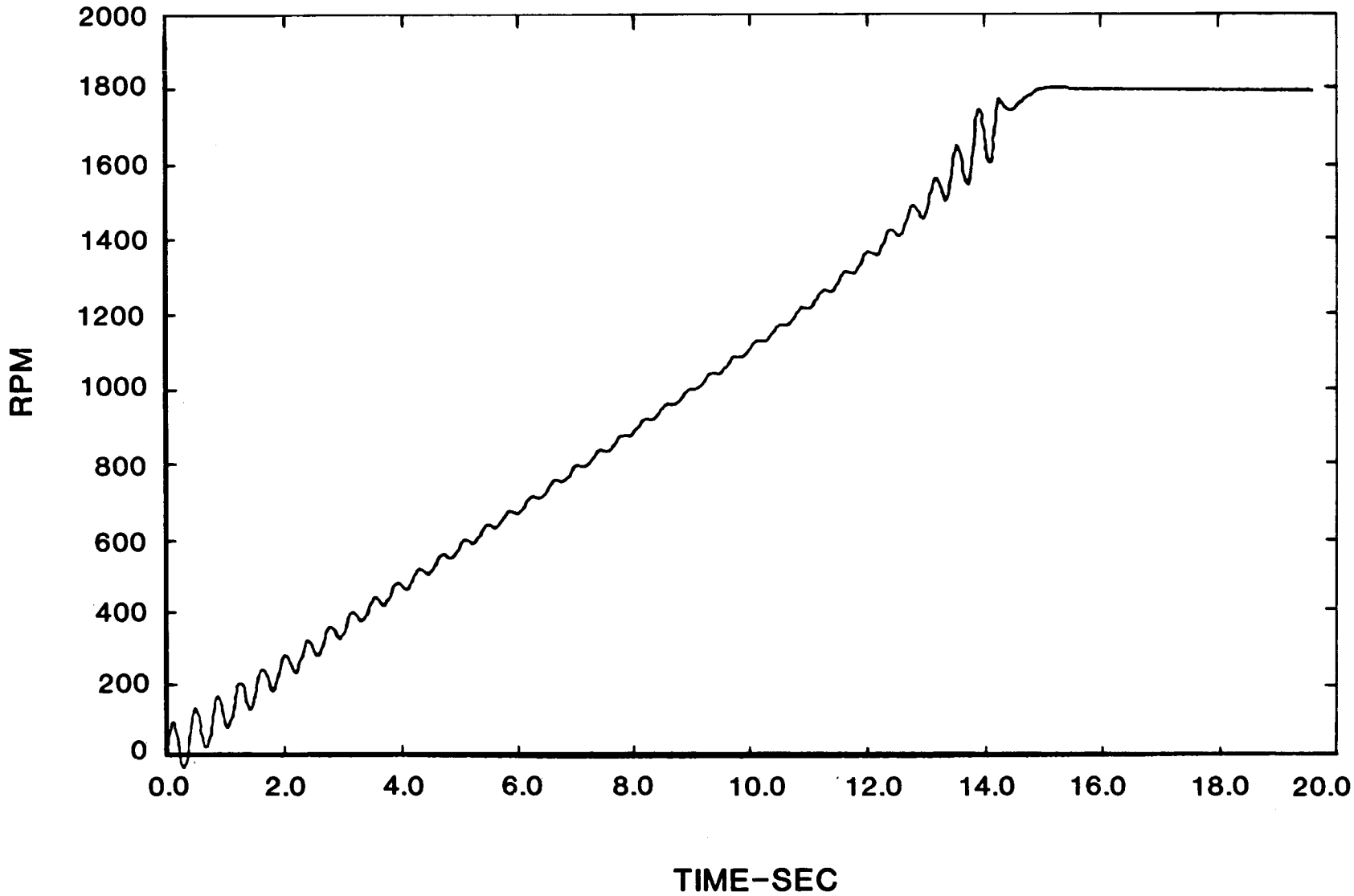

Figure 14. DYDTA prediction - Motor speed vs. time for start-up in zero wind - no clutch.

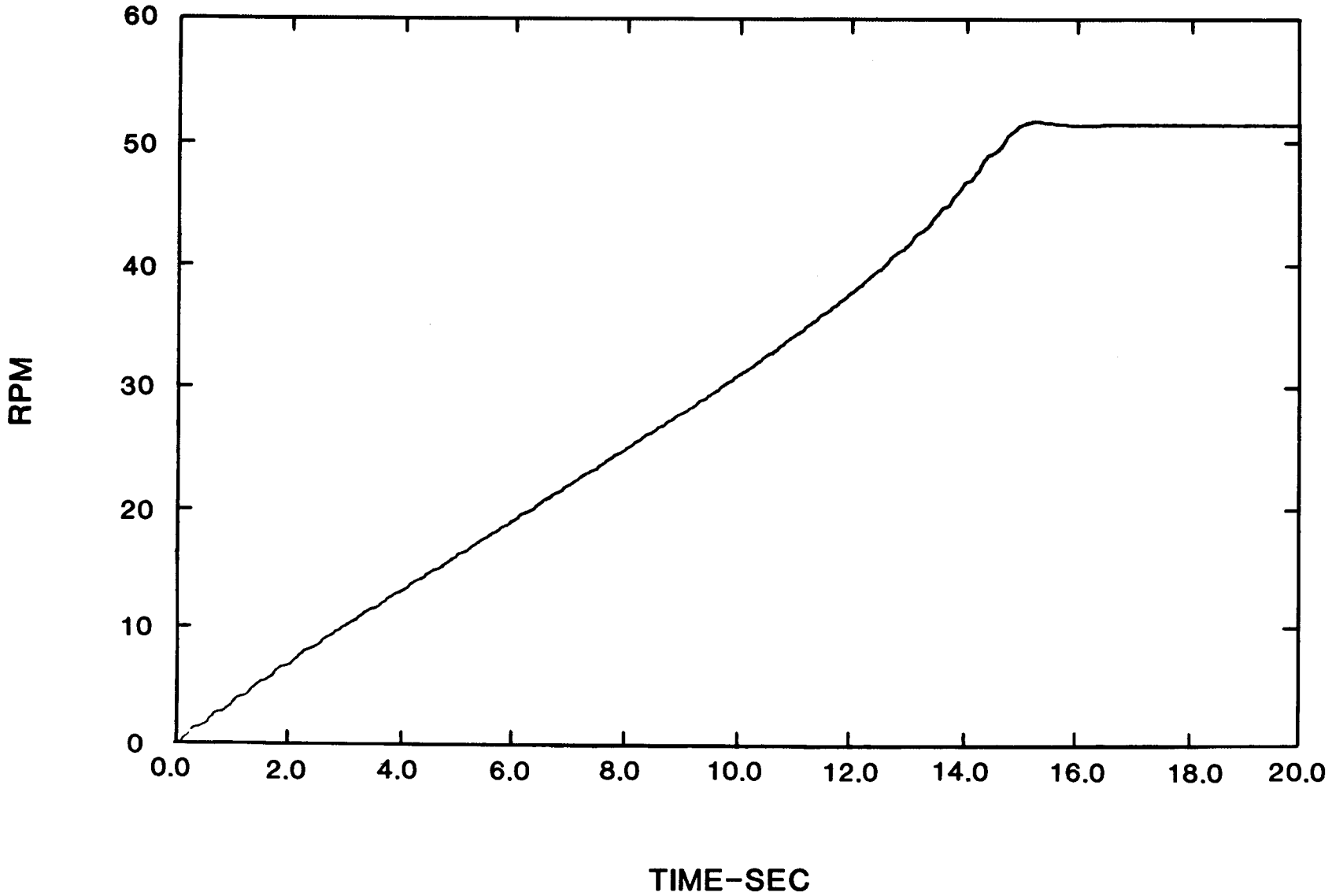

Figure 15. DYDTA prediction - Rotor speed vs. time for start-up in zero wind - no clutch.

corresponds to an 18% voltage drop in the line. This is not unreasonable as the current drawn by the motor is rather high and the line is fairly long at the Rocky Flats site. Obviously the scale factor depends on the particular motor and electrical arrangement for a given VAWT design. The viscous damping coefficient was determined to be 1.1×10^3 lb-ft-sec, corresponding to a damping factor of approximately one percent. This is insignificant compared to damping provided by the motor and thus the influence of viscous damping due to the structure on the response is negligible.

The results from DYDTA, after adjustment of the scale factor and viscous damping coefficient, show excellent agreement with the field data (Figure 11), and the simple drive train model can be used to explain the characteristics typical of a VAWT start-up in zero wind. DYDTA correctly predicts the magnitude of the initial overshoot and the subsequent decay. The initial overshoot is due to the step in torque which occurs when the motor is turned on; the amplitude should be approximately twice the initial motor torque (locked rotor torque). When the motor speed is less than the pull-up speed (725 rpm) the motor contributes a small amount of positive damping, and together with the viscous damping due to the structure it causes the oscillations to decay in the typical envelope fashion. However, the rate of decay constantly decreases and eventually becomes zero as the damping from the motor goes from positive at locked rotor to zero at pull-up and becomes negative beyond that.

The growth of torque oscillations occurs when the damping produced by the motor becomes negative, an effect also predicted by DYDTA, Figure 12. Negative damping results in energy addition to the system, which causes an unstable growth in the amplitude of the torque oscillations. The maximum torque seen by the low speed shaft occurs at approximately the time the motor breakdown speed is reached, when the motor damping changes rapidly from negative to positive. As

explained earlier, there is a frequency shift at this point as well: prior to breakdown, the total damping is relatively small, and thus it does not significantly affect the 1st fundamental frequency. Since the rotor inertia is much larger than the motor/brake inertia, the vibrational mode basically consists of the motor/brake winding up on the low speed shaft. Past breakdown the large positive damping produced by the motor effectively reduces the motor/brake vibration to zero, so that the first mode shape becomes the rotor oscillating about the low speed shaft. There is a significant decrease in the fundamental vibrational frequency past breakdown due to the large size of the rotor inertia relative to that of the motor/brake. Again, DYDTA is in very good agreement with field data with regard to these phenomena. DYDTA also matches experimental records on starting times, which essentially depends on rotor inertia and mean motor torque.

Figure 13 demonstrates the variation of motor torque as a function of time, which is another critical aspect of VAWT start-up. Up until breakdown the motor draws very high levels of current, and the motor can draw high power for only a short period of time. Past breakdown the current is reduced, so it is clearly advantageous to reduce the time to breakdown (t_{BD}) as much as possible. For the base case t_{BD} is about 14.7 seconds. Figures 14 and 15 show the speeds of the motor/brake and rotor, respectively as functions of time. They serve to verify that the turbine successfully comes up to speed, as well as to substantiate what has been said earlier in regard to the mode shapes (the rotor motion is almost entirely a rigid body mode whereas the motor contains a significant amount of oscillation about the rigid body mode).

Control of Transients with a Slip Clutch

High torques experienced in the low speed shaft of the Low Cost 17M turbine resulted in the investigation of a slip clutch

as a possibility for reducing peak torques. DYDTA has been used to analyze the effect of a slip clutch on torque levels during start-up. The results indicate a clutch could significantly lower the peak torques seen by the low speed shaft, with the following secondary benefit. The clutch also reduces the time to breakdown for the motor (t_{BD}), which reduces the current drawn by the motor and protects it from overload. It appears that an appropriately chosen clutch would be well within margins of safety with respect to heat dissipation and power absorption capabilities.

The characteristics of a typical slip clutch were discussed earlier; recall that the clutch passes torque uniformly up to some maximum value (T_{max}) which can be adjusted by changing the deflection of a compression spring. With this in mind a parametric study was done using DYDTA to determine what value or range of T_{max} would best reduce torque levels. Obviously T_{max} should be above the rated turbine torque, which is 427 ft-lbs (15,000 ft-lbs referred to the low speed shaft), or else power could be absorbed by the clutch during normal operation.

The optimum value for T_{max} for the Low Cost turbine appears to be 475 ft-lbs (16,700 ft-lbs referred to the low speed shaft), for which the results predicted by DYDTA are shown in Figures 16-21. With the clutch present, the maximum torque in the low speed shaft occurs during the initial overshoot, and its magnitude has been reduced 38% from 40,000 ft-lbs to 25,000 ft-lbs. The growth of torque oscillations does not occur because slipping of the clutch decouples the motor from the drive train, thereby isolating the low speed shaft from the negative damping produced by the motor. Note that the torque in the low speed shaft can exceed T_{max}, despite the clutch, because of the inertial reaction of the brake. This implies that the slip clutch should be located as close to the component needing protection as is physically possible.

The clipping action of the clutch is demonstrated in Figure 17; the torque transmitted through the clutch cannot exceed

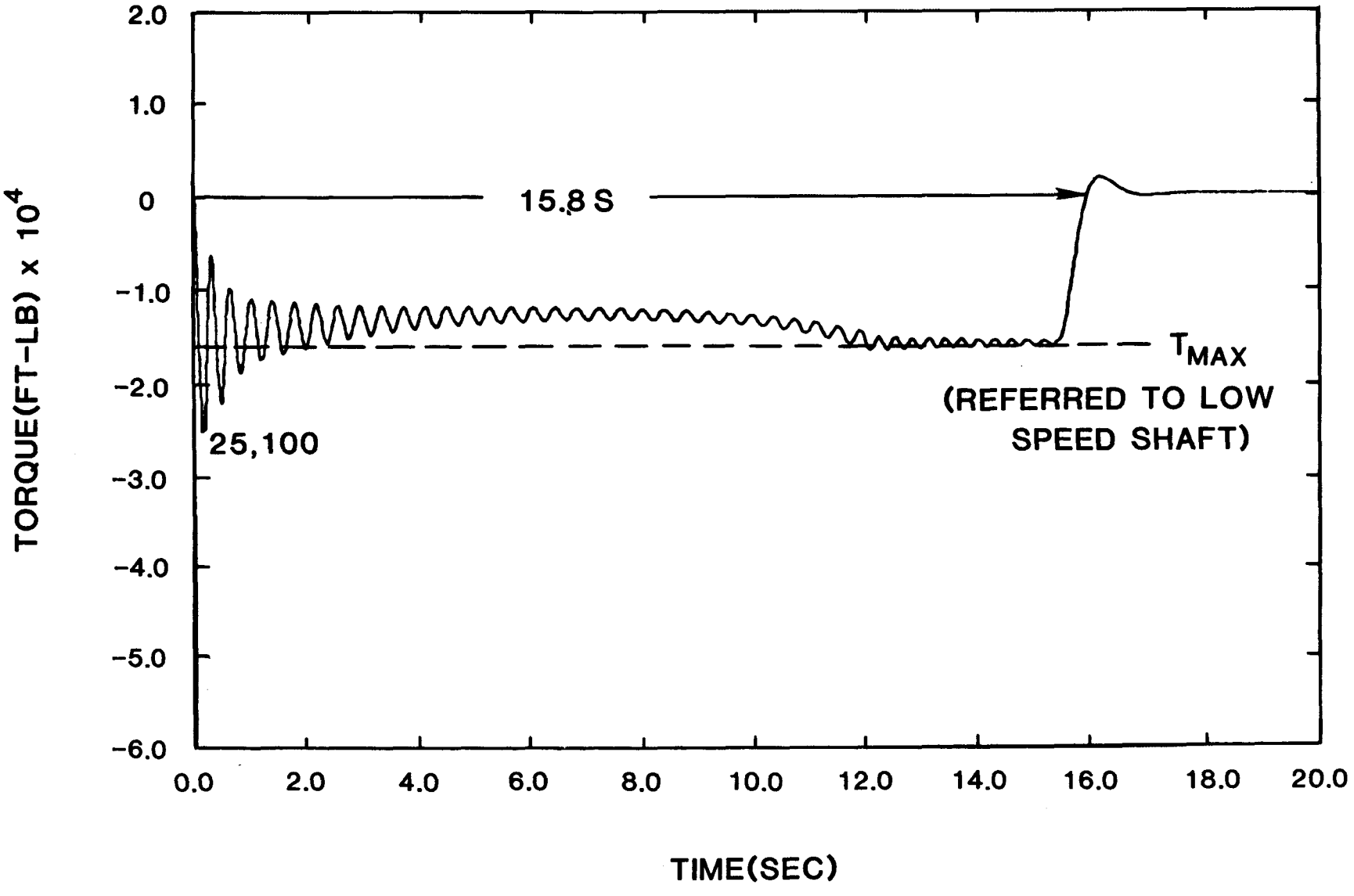

Figure 16. DYDTA prediction - Low speed shaft torque vs. time during start-up in zero wind with clutch.

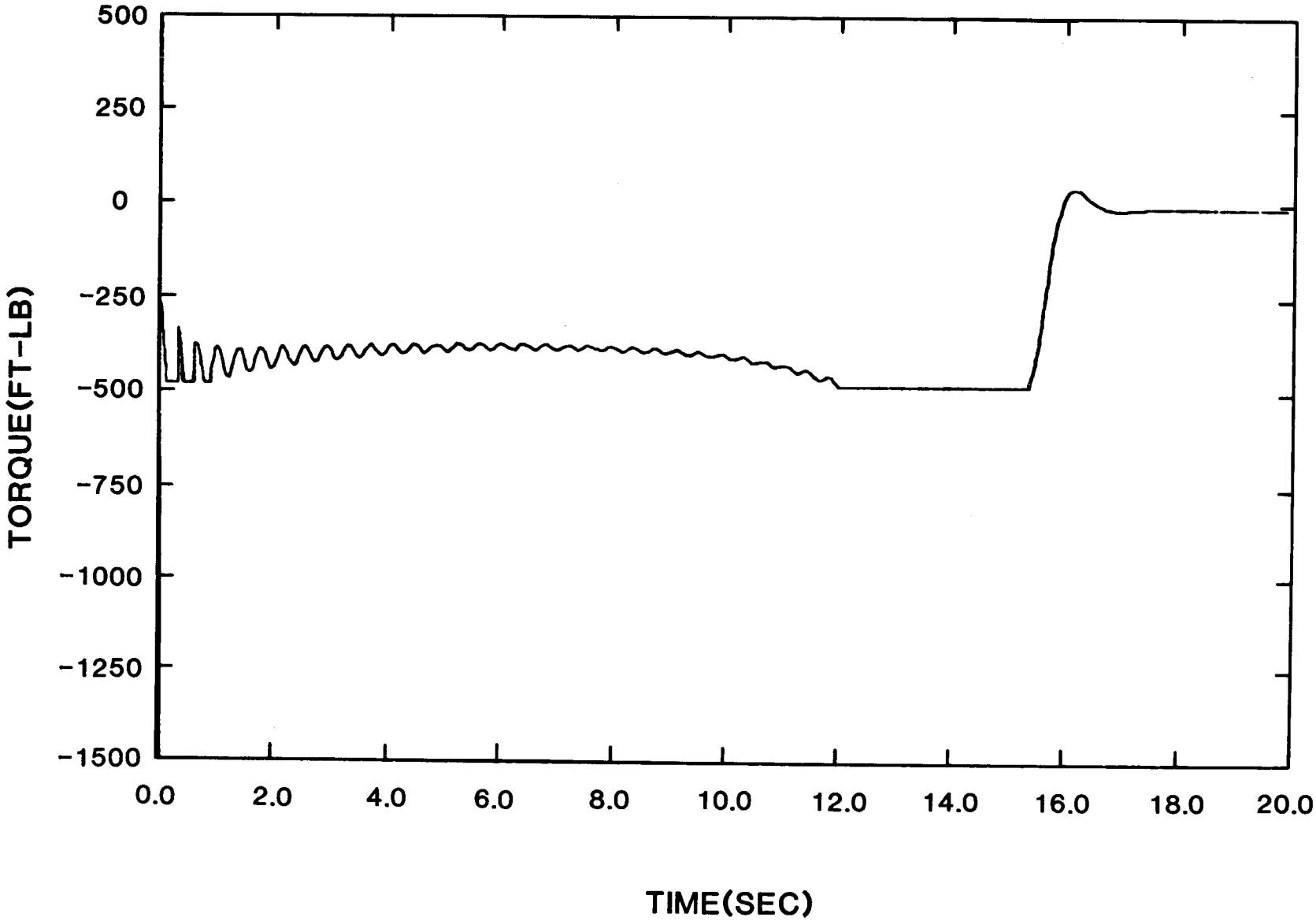

Figure 17. DYDTA prediction - Torque transmitted through clutch vs. time during start-up in zero wind with clutch.

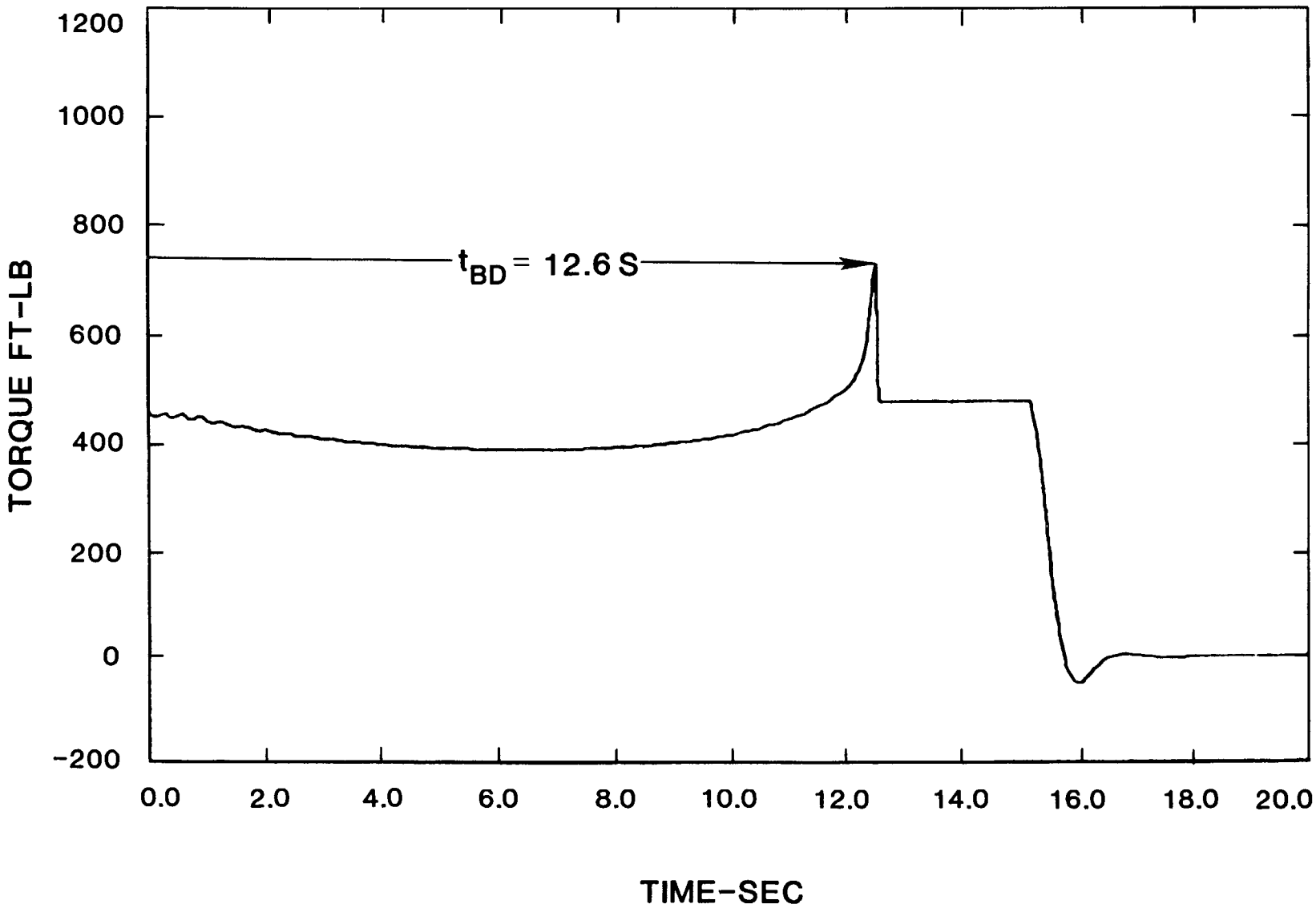

Figure 18. DYDTA prediction - Motor torque vs. time for start-up in zero wind with clutch.

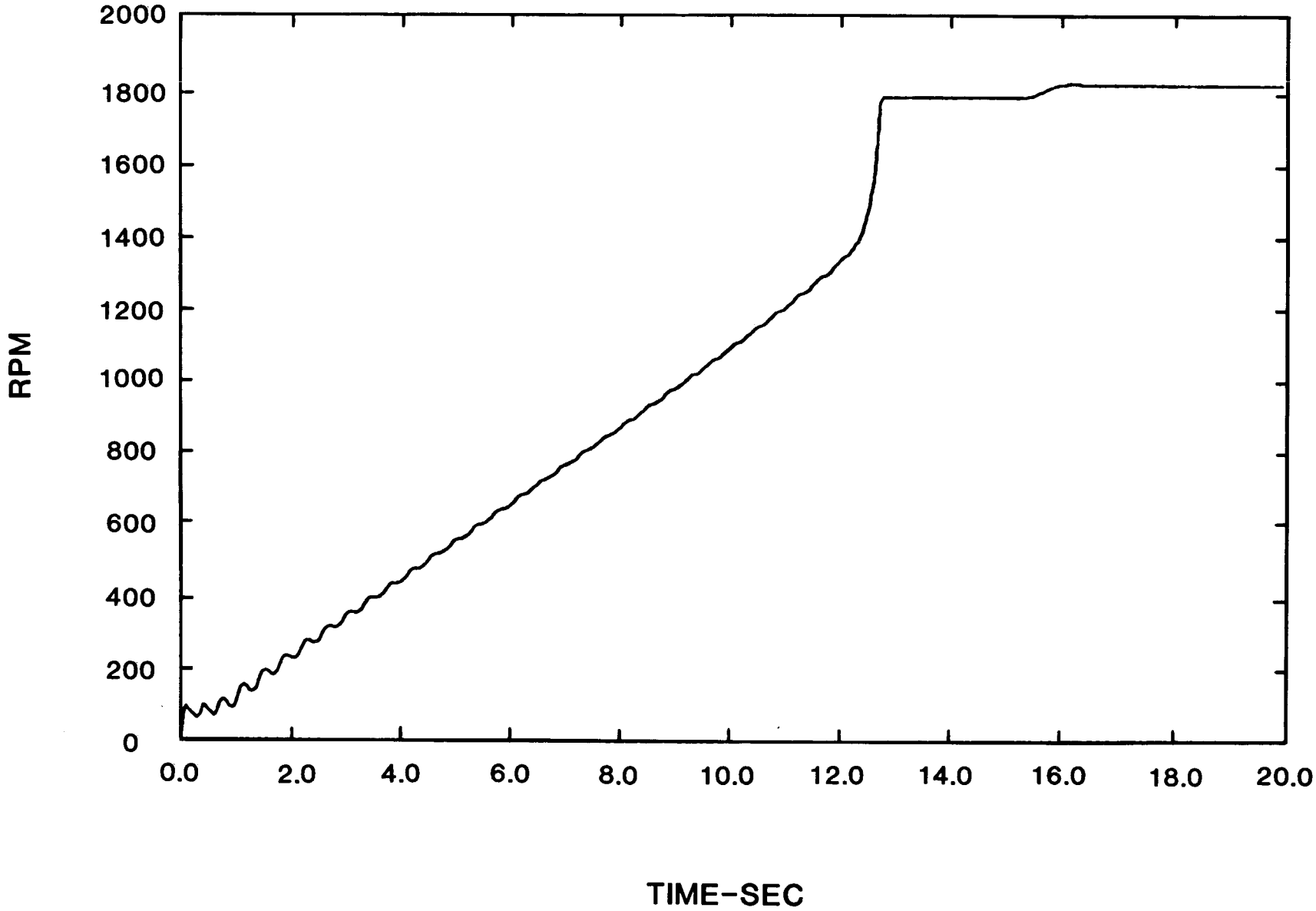

Figure 19. DYDTA prediction - Motor speed vs. time for start-up in zero wind with clutch.

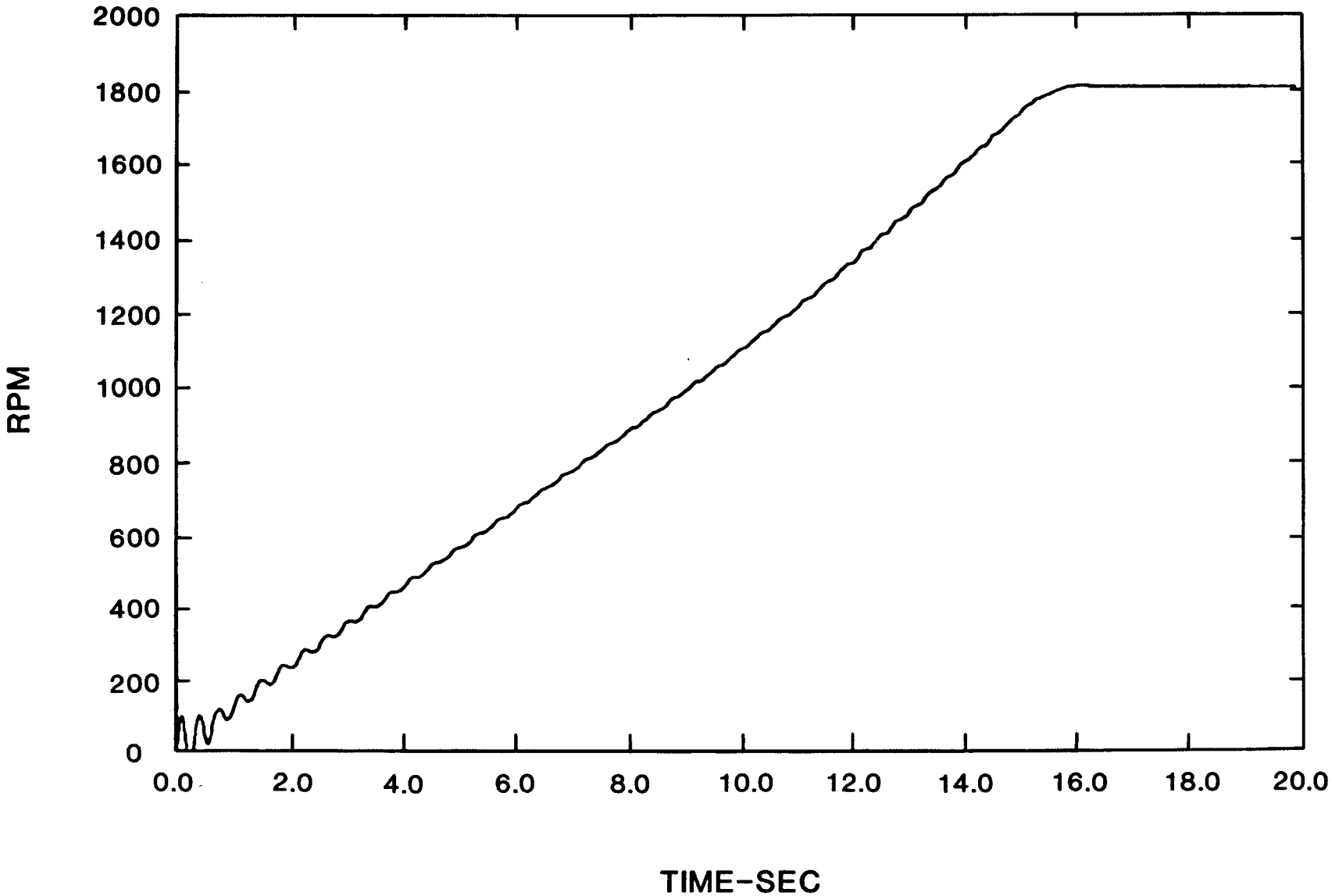

Figure 20. DYDTA prediction - Clutch speed (rotor side) vs. time for start-up in zero wind.

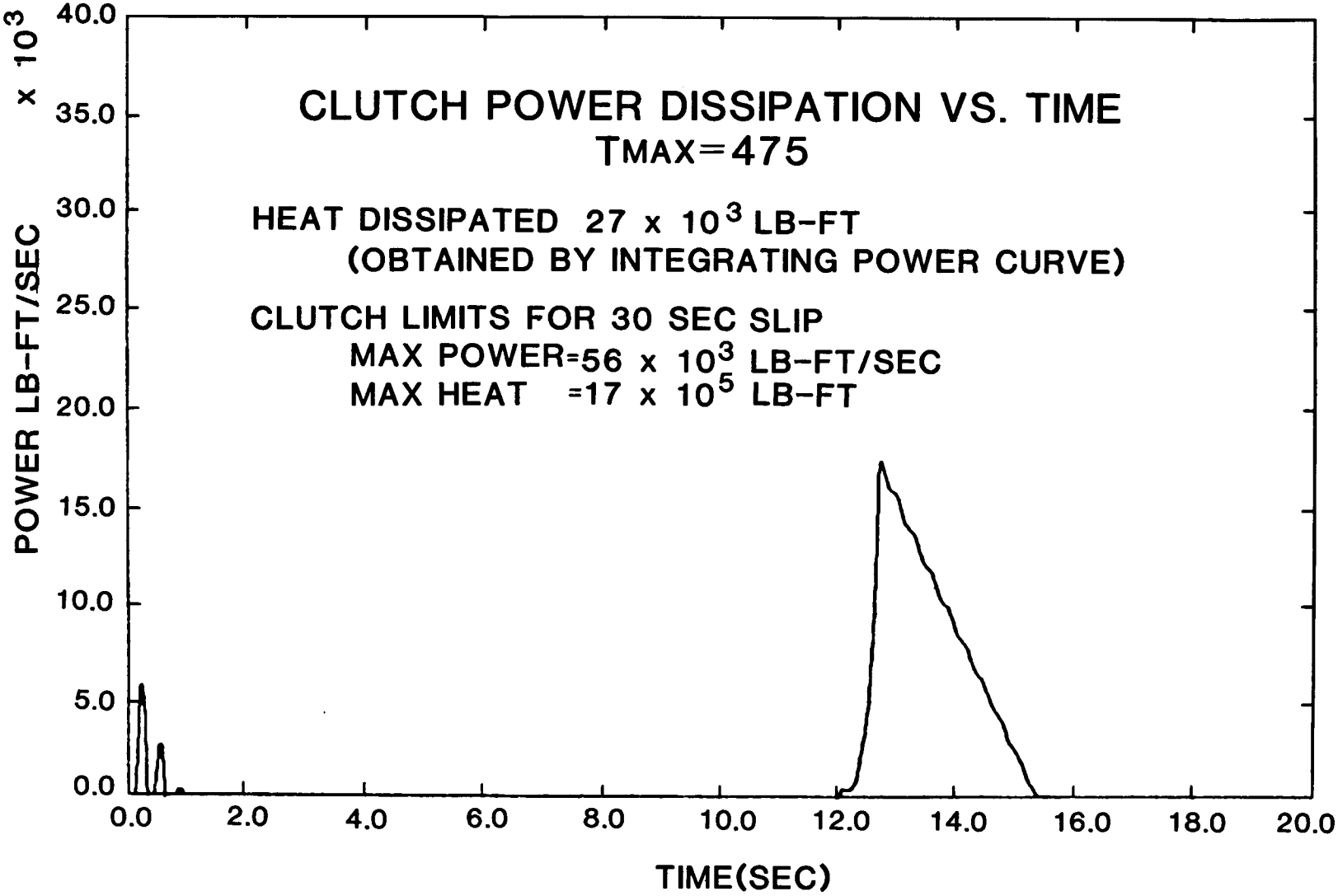

Figure 21. DYDTA prediction - Power dissipated in clutch vs. time for start-up in zero wind.

T_{max}. As discussed previously, a secondary benefit is that the clutch reduces t_{BD} for the motor. Figure 18 shows that the high torque part of the motor curve is sped through very rapidly, and t_{BD} is reduced to 12.6s from 14.7s for no clutch. Figures 19 and 20 can be compared to determine at what times the clutch is slipping. The power dissipated in the clutch as a function of time, and the total heat dissipated (obtained by integrating the power curve) are shown in Figure 21.

Conclusions

DYDTA represents an initial step towards understanding and analyzing methods of controlling transient behavior in VAWT drive trains. Results for start-up in zero wind speed show exceptional agreement with experimental records on the Low Cost 17M turbine, thus providing verification of modeling accuracy. DYDTA is currently being used to predict responses for several different transient operations and possible design modifications intended to reduce transient torque levels. It is expected to become a versatile, easily implemented drive train design tool.

Acknowledgments

The assistance of the following is gratefully acknowledged: T. M. Leonard for his programming ideas and support, P. S. Veers and K. W. Schuler for their help towards understanding and describing the slip clutch, and W. N. Sullivan for the initiation of this project.

References

1. Reuter, R. C., "Torque Ripple in a Darrieus Vertical Axis Wind Turbine," Sandia National Laboratories Report No. SAND80-0475, September 1980.

2. Mirandy, L. P., "Rotor/Generator Isolation for Wind Turbines," Journal of Energy, Vol. 1, No. 3, May-June, 1977.

Appendix A
Description of Computer Code DYDTA

DYDTA, DYnamic Drive Train Analysis, is a Fortran code which is intended primarily for solution of the transient dynamics problems associated with VAWT drive trains. The inherent phenomenon associated with steady state operation of a VAWT called torque ripple can also be studied with the code, although at this time the method developed by Reuter [1] is recommended. The code is presently in a state of development, and complete documentation will be published at a later date.

DYDTA is capable of obtaining the solution for any feasible drive train topology, whereas the solution approach taken in this paper is a special case. The number of different configurations of a VAWT drive train are relatively small because the locations of the rotor and generator are essentially fixed. The capability to solve different topologies is a very powerful tool because it enables comparative studies of high speed vs. low speed brakes, as well as the relative effectiveness of a clutch in differing locations in the drive train. The equations of motion are written based on a lumped parameter model of the structure, and solved using ODE (Ordinary Differential Equations), a library subroutine which performs numerical integration. A slip clutch and timing belt are included in the model for generality, however, the user can negate the effect of these components with appropriate choice of input. For example, by inputting a very large value for the maximum torque transmitted by the slip clutch its effect will be negated, since the maximum torque will not be reached and the clutch will not slip.

The code is written to be fully user-interactive; the user is prompted for all input. Required input includes mechanical properties of the system (inertia, damping and stiffness), gear ratios, and a code number for the desired drive train topology. The user must also input information which characterizes the applied torques (motor, brake, and/or aerodynamic) which are to be considered. Typically this consists of inputting several points of torque vs. speed and/or time data. Optional input includes the initial conditions and the integration parameters, although default values exist. Output can be in either tabular or plot form, and the amount of information is controlled by user input. Available output includes speed, torque, and power as functions of time in all relevant mechanical components.

Appendix B

Behavior of a Slip Clutch

In order to understand the behavior of a slip clutch and the consequences of the mathematical modeling of the clutch, it is instructive to examine in detail the response of a two degree-of-freedom system which contains a slip clutch. This system is sufficiently simple that it can be solved analytically, thus allowing a more complete understanding of its response. The system we wish to examine is diagrammed in Figure B1 with the indicated notation. The applied torque is constant and represented by T_o. The torsional spring has a spring constant of K, and the clutch torque, T_c has a maximum value of T_{max}.

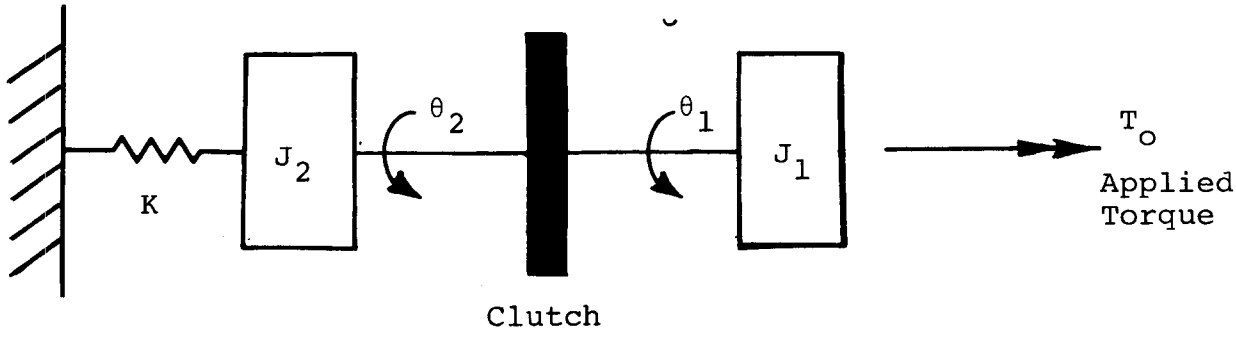

FIGURE B1. DIAGRAM OF TWO DEGREE-OF-FREEDOM SYSTEM

There are two operating states for the clutch, engagement and slip, as discussed earlier. The equations of motion for this system for the two states are given below.

Engagement Equations

$$(J_1 + J_2)\ddot{\theta}_2 + K\theta_2 = T_o \quad , \tag{B1}$$

$$\dot{\theta}_1 = \dot{\theta}_2 \quad , \tag{B2}$$

$$|T_c| \leq T_{max} \quad , \tag{B3}$$

$$T_c = T_o - J_1\ddot{\theta}_1 \tag{B4}$$

Slip Equations

$$J_1\ddot{\theta}_1 = T_o - T_c \quad , \tag{B5}$$

$$J_2\ddot{\theta}_2 + K\theta_2 = T_c \quad , \tag{B6}$$

$$T_c = \pm T_{max} \quad . \tag{B7}$$

In order to solve these equations in a simple form so as to observe the behavior of the clutch, we can use the homogeneous initial conditions

$$\theta_1(0) = \theta_2(0) = 0 \text{ and } \dot{\theta}_1(0) = \dot{\theta}_2(0) = 0 \quad , \tag{B8}$$

and let $T_{max} = 1.25\ T_o$ (B9)

and set $J_1 = J_2$. (B10)

At t=0 there is no slipping of the clutch and the engagement equations apply. Equations (B1), (B2) and the initial conditions (B8) produce the solution

$$\theta_1 = \frac{T_o}{K}(1-\cos\omega_1 t), \quad \omega_1 = \sqrt{\frac{K}{J_1 + J_2}} \quad , \tag{B11}$$

and $\theta_2 = \theta_1$, $0 < t < t_s$.

These solutions apply as long as the clutch stays engaged. The point in time, t_s, at which the clutch starts to slip, if ever, can be computed from the clutch torque equation (B4),

$$T_c = T_o - J_1\ddot{\theta}_1 \ .$$

Using (B11) and (B10)

$$T_c = T_o(1 - \frac{1}{2}\cos\omega_1 t) \ . \qquad \text{(B12)}$$

We see in (B12) that the clutch torque initially has a value of $T_o/2$ and then increases with time. The clutch torque would have a maximum value of 1.5 T_o except that it exceeds T_{max}, so the clutch will start to slip before that point. To find the time at which the clutch slips, t_s, we use (B9) in the above equation to find

$$t_s = \frac{2}{3}\,\pi/\omega_1 \ . \qquad \text{(B13)}$$

Thus, the clutch starts to slip when $t = \frac{2}{3}\pi/\omega_1$. If the clutch did not exist, then θ_1 and θ_2 would continue to be equal and increase as in (B11), reaching their maximum value of $2T_o/K$ at $t = \pi/\omega_1$. However, for $t > t_s$ the slip equations apply until reengagement occurs when $\dot{T}_c \leq 0$ and $\dot{\theta}_1 = \dot{\theta}_2$.

Using (B11) and (B13), new initial conditions can be computed for the slip equations of motion.

$$\begin{aligned} \theta_1(t_s) &= \theta_2(t_s) = \frac{3}{2}\,\frac{T_o}{K} \ , \text{ and} \\ \dot{\theta}_1(t_s) &= \dot{\theta}_2(t_s) = \frac{\sqrt{3}}{2}\,\omega_1\,\frac{T_o}{K} \ . \end{aligned} \qquad \text{(B14)}$$

Now applying the slip equations (B5), (B6), and (B7) with $T_c = + T_{max}$, we find

$$\begin{aligned} J_1\ddot{\theta}_1 &= -\frac{1}{4}\,T_o \ , \text{ and} \\ J_2\ddot{\theta}_2 + K\theta_2 &= \frac{5}{4}\,T_o \ . \end{aligned} \qquad \text{(B15)}$$

These equations show a key behavior of the clutch. Up to this point of time, t_s, $\theta_1 = \theta_2$. However, when the clutch is

slipping, $\ddot{\theta}_1 \neq \ddot{\theta}_2$, consequently the velocities and angles no longer remain equal. Solving the equations (B15) with the initial conditions (B14), we find

$$\theta_1 = \frac{T_o}{K}\left[-\frac{1}{8}\omega_2^2 (t-t_s)^2 + \frac{\sqrt{3}}{2}\omega_1 (t-t_s) + \frac{3}{2}\right] ,$$

and

$$\theta_2 = \frac{T_o}{K}\left[\frac{1}{4}\cos\omega_2(t-t_s) + \frac{\sqrt{6}}{4}\sin\omega_2(t-t_s) + \frac{5}{4}\right] , \qquad \text{(B16)}$$

for all t, $t_s \leq t \leq t_e$, where $\omega_2 = \sqrt{\frac{K}{J_2}}$

and t_e indicates the time when reengagement occurs, if ever.

The algebra at this point in the analysis is getting sufficiently involved so as to obscure the physics. Consequently, it is best to turn now to a plot of the solution. Figure B2 shows the two angles, the two angular velocities, and the clutch torque all plotted as functions of time. Examining the figure, one can see the point at which the clutch starts to slip and when it reengages. When the clutch is slipping, the angular velocities are no longer equal. However, the clutch is applying a torque in the direction so as to equalize the velocities again. This happens at t_e when the velocities are again equal and the clutch engages. Note also the behavior of the clutch torque. While the clutch is slipping, $T_c = T_{max}$; when the clutch is engaged, $T_c < T_{max}$. One can also observe from the figure the discontinuity in $\ddot{\theta}_1$ and $\ddot{\theta}_2$ when the clutch reengages.

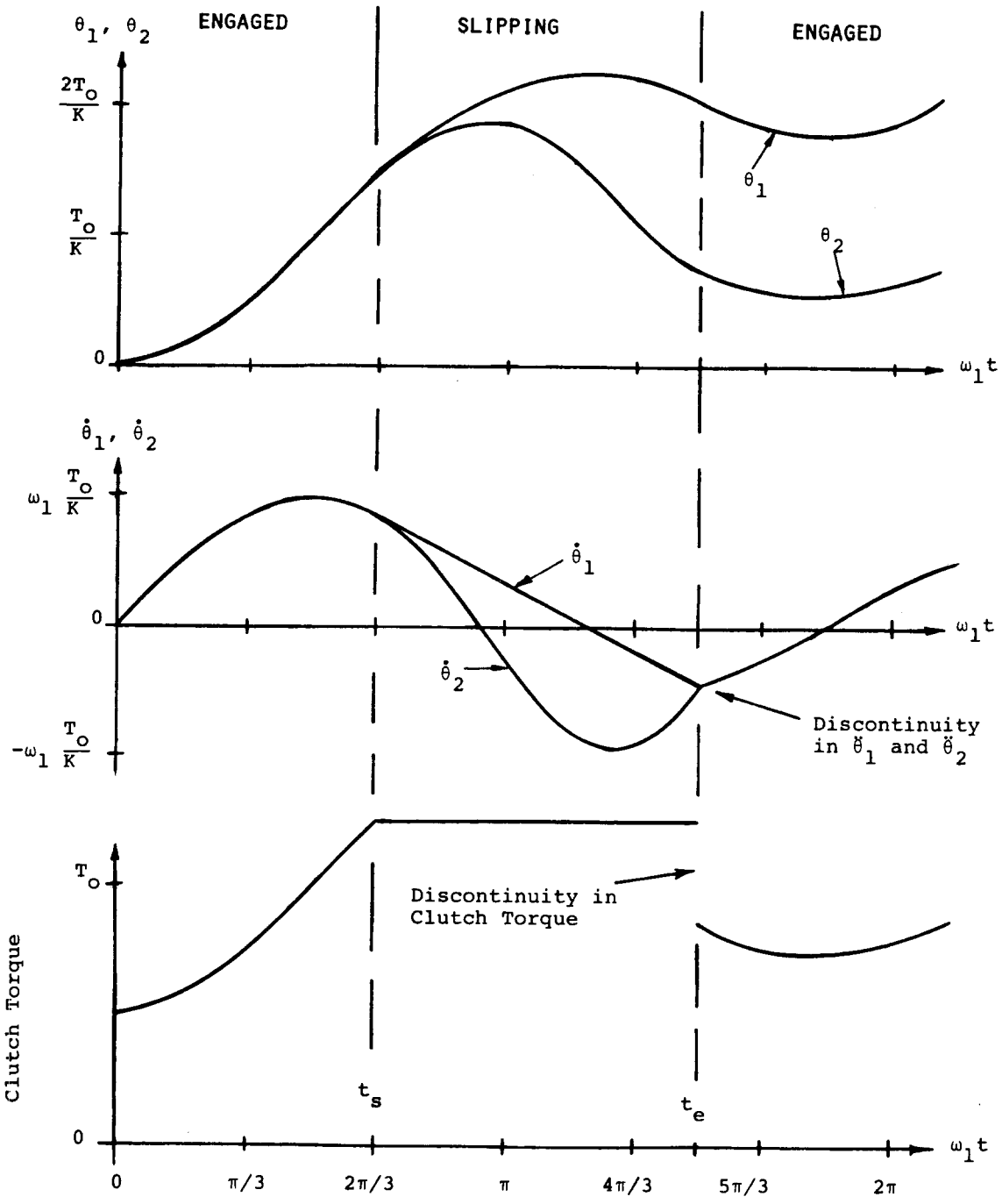

FIGURE 2B. RESPONSE OF TWO DEGREE-OF-FREEDOM SYSTEM

DISTRIBUTION:

TID-4500-R66 UC-60 (283)

Aero Engineering Department (2)
Wichita State University
Wichita, KS 67208
Attn: M. Snyder
W. Wentz

R. E. Akins, Assistant Professor
Department of Engineering Science
and Mechanics
Virginia Polytechnic Institute and
State University
Blacksburg, VA 24060

Alcoa Laboratories (5)
Alcoa Technical Center
Aluminum Company of America
Alcoa Center, PA 15069
Attn: D. K. Ai
A. G. Craig
J. T. Huang
J. R. Jombock
P. N. Vosburgh

Mr. Robert B. Allen
General Manager
Dynergy Corporation
P.O. Box 428
1269 Union Avenue
Laconia, NH 03246

American Wind Energy Association
1609 Connecticut Avenue NW
Washington, DC 20009

E. E. Anderson
South Dakota School of Mines
and Technology
Department of Mechanical
Engineering
Rapid City, SD 57701

Scott Anderson
318 Millis Hall
University of Vermont
Burlington, VT 05405

G. T. Ankrum
DOE/Office of Commercialization
20 Massachusetts Avenue NW
Mail Station 2221C
Washington, DC 20585

Holt Ashley
Stanford University
Department of Aeronautics and
Astronautics Mechanical Eng
Stanford, CA 94305

Kevin Austin
Consolidated Edison Company of
New York, Inc.
4 Irving Place
New York, NY 10003

B. H. Barksdale, Jr.
Hayes, Seay, Mattern, and Mattern
1315 Franklin Road SW
Roanoke, VA 24016

Dr. P. J. Baum
Institute of Geophysics
and Planetary Physics
University of California
Riverside, CA 92521

F. K. Bechtel
Washington State University
Department of Electrical Eng
College of Engineering
Pullman, WA 99163

M. E. Beecher
Arizona State University
Solar Energy Collection
University Library
Tempe, AZ 85281

Leon Bjervig
Civilingenior, MCIF
"Osterbyhus", 6990 Ulfborg
DK6990
DENMARK

K. Bergey
University of Oklahoma
Aero Engineering Department
Norman, OK 73069

Steve Blake
Wind Energy Systems
Route 1, Box 93-A
Oskaloosa, KS 66066

Robert Brulle
McDonnell-Douglas Aircraft Corp
P.O. Box 516
Department 341, Building 32/2
St. Louis, MO 63166

R. Camerero
Faculty of Applied Science
University of Sherbrooke
Sherbrooke, Quebec
CANADA J1K 2R1

CERCEM
49 Rue du Commandant Rolland
93350 Le Bourget
FRANCE
Attn: G. Darrieus
J. Delassus

Professor V. A. L. Chasteau
School of Engineering
University of Auckland
Private Bag
Auckland, NEW ZEALAND

Howard T. Clark
McDonnell Aircraft Corporation
P.O. Box 516
Department 337, Building 32
St. Louis, MO 63166

Dr. R. N. Clark
USDA, Agricultural Research Service
Southwest Great Plains Research Center
Bushland, TX 79012

Joan D. Cohen
Consumer Outreach Coordinator
State of New York
Executive Department
State Consumer Protection Board
99 Washington Avenue
Albany, NY 12210

Dr. D. E. Cromack
Associate Professor
Mechanical and Aerospace Eng Department
University of Massachusetts
Amherst, MA 01003

Gale B. Curtis
Tumac Industries
650 Ford Street
Colorado Springs, CO 80915

DOE/ALO (2)
Albuquerque, NM 87115
Attn: G. P. Tennyson
D. W. King

DOE Headquarters/WESD (20)
600 E Street NW
Washington, DC 20545
Attn: D. F. Ancona
C. E. Aspliden
L. V. Divone
W. C. Reddick

C. W. Dodd
School of Engineering
Southern Illinois University
Carbondale, IL 62901

D. D. Doerr
Kaiser Aluminum and Chemical Sales, Inc.
6177 Sunol Blvd.
P.O. Box 877
Pleasonton, CA 94566

Dominion Aluminum Fabricating Ltd. (2)
3570 Hawkestone Road
Mississauga, Ontario
CANADA L5C 2U8
Attn: L. Schienbein
C. Wood

D. P. Dougan
Hamilton Standard
1730 NASA Boulevard
Room 207
Houston, TX 77058

J. B. Dragt
Nederlands Energy Research Foundation (E.C.N.)
Physics Department
Westerduinweg 3 Patten (nh)
THE NETHERLANDS

C. E. Elderkin
Battelle-Pacific Northwest Laboratory
P.O. Box 999
Richland, WA 99352

Frank R. Eldridge, Jr.
The Mitre Corporation
1820 Dolley Madison Blvd.
McLean, VA 22102

Electric Power Research Institute
3412 Hillview Avenue
Palo Alto, CA 94304
Attn: E. Demeo

Richard G. Ferreira, Chief
The Resources Agency
Department of Water Resources
Energy Division
1416 9th Street
P.O. Box 388
Sacremento, CA 95802

D. R. Finley
New England Geosystems
P.O. Box 128
East Derry, NH 03041

James D. Fock, Jr.
Department of Aerospace
Engineering Sciences
University of Colorado
Boulder, CO 80309

Dr. Lawrence C. Frederick
Public Service Company of
New Hampshire
1000 Elm Street
Manchester, NH 03105

H. Gerardin
Mechanical Engineering Department
Faculty of Sciences and Eng.
Universite Laval-Quebec
CANADA G1K 7P4

E. Gilmore
Amarillo College
Amarillo, TX 79100

Paul Gipe
Wind Power Digest
P.O. Box 539
Harrisburg, PA 17108

Roger T. Griffiths
University College of Swansea
Department of Mechanical Eng.
Singleton Park
Swansea SA2 8PP
UNITED KINGDOM

A. A. Hagman
Kaiser Aluminum and Chemical
Sales, Inc.
14200 Cottage Grove Avenue
Dolton, IL 60419

Martin L. Hally, Section Manager
Project Department
Electricity Supply
18 St. Stephen's Green
Dublin 2, IRELAND

Professor N. D. Ham
Massachusetts Institute
of Technology
77 Massachusetts Avenue
Cambridge, MA 02139

Sam Hansen
DOE/DST
20 Massachusetts Avenue
Washington, DC 20545

C. F. Harris
Wind Engineering Corporation
of Technology
Airport Industrial Area
Box 5936
Lubbock, TX 79415

W. L. Harris
Aero/Astro Department
Massachusetts Institute
Cambridge, MA 02139

Terry Healy (2)
Rockwell International
Rocky Flats Plant
P.O. Box 464
Golden, CO 80401

Helion
P.O. Box 4301
Sylmar, CA 91342

Don Hinrichsen
Associate Editor
AMBIO
KVA
Fack, S-10405
Stockholm
SWEDEN

Sven Hugosson
Box 21048
S. 100 31 Stockholm 21
SWEDEN

O. Igra
Department of Mechanical Eng
Ben-Gurion University of the Negev
Beer-Sheva, ISRAEL

Indian Oil Corporation, Ltd.
Marketing Division
254-C, Dr. Annie Besant Road
Prabhadevi, Bombay-400025
INDIA

JBF Scientific Corportion
2 Jewel Drive
Wilmington, MA 01887
Attn: E. E. Johanson

Dr. Gary L. Johnson, P.E.
Electrical Engineering Department
Kansas State University
Manhattan, KS 66506

B. C. Kaddy, Jr.
Box 353
31 Union Street
Hillsboro, NH 03244

Kaman Aerospace Corporation
Old Windsor Road
Bloomfield, CT 06002
Attn: W. Batesol

R. L. Katzenberg
2820 Upton St. NW
Washington, DC 20008

Robert E. Kelland
The College of Trades and
Technology
P.O. Box 1693
Prince Philip Drive
St. John's, Newfoundland
CANADA A1C 5P7

S. King
Natural Power, Inc.
New Boston, NH 03070

Larry Kinnett
P.O. Box 6593
Santa Barbara, CA 93111

Samual H. Kohler
272 Old Delp Road
Lancaster, PA 17602

O. Krauss
Michigan State University
Division of Engineering Research
East Lansing, MI 48824

Carol Lamb
2584 East Geddes Avenue
Littleton, CO 80122

Lawrence Livermore Laboratory
P.O. Box 808 L-340
Livermore, CA 94550
Attn: D. W. Dorn

M. Lechner
Public Service Company
of New Mexico
P.O. Box 2267
Albuquerque, NM 87103

Kalman Nagy Lehoczky
Cort Adelers GT. 30
Oslo 2
NORWAY

George E. Lennox
Industry Director
Mill Products Division
Reynolds Metals Company
6601 West Broad Street
Richmond, VA 23261

J. Lerner
State Energy Commission
Research and Development Division
1111 Howe Avenue
Sacramento, CA 95825

L. Liljidahl
Building 303
Agriculture Research Center
USDA
Beltsville, MD 20705

P. B. S. Lissaman
Aeroenvironment, Inc.
660 South Arroyo Parkway
Pasadena, CA 91105

Olle Ljungstrom
FFA, The Aeronautical Research
Institute
Box 11021
S-16111 Bromma
SWEDEN

T. H. Logan
U.S. Turbine Corporation
Olde Courthouse Building
Canfield, OH 44406

J. B. Longendyck
Siltex
7 Capitol Drive
Moonachie, NJ 07074

Los Alamos Scientific Laboratories
P.O. Box 1663
Los Alamos, NM 87544
Attn: J. D. Balcomb Q-DO-T

Beatrice de Saint Louvent
Establissement d'Etudes et de
Meteorologigues
77, Rue de Serves
92106 Boulogne-Billancourt Cedex
Recherches
FRANCE

Ernel L. Luther
Senior Associate
PRC Energy Analysis Co.
7600 Old Springhouse Rd.
McLean, VA 22101

L. H. J. Maile
48 York Mills Rd.
Willowdale, Ontario
CANADA M2P 1B4

E. L. Markowski
Motolola, Inc.
G.E.D.
Mail Drop 1429
8201 E. McDowell Rd.
P.O. Box 1417
Scottsdale, AZ 85252

Jacques R. Maroni
Ford Motor Company
Environmental Research and Energy
Planning Director
Environmental and Safety
Engineering Staff
The American Road
Dearborn, MI 48121

Frank Matanzo
Dardalen Associates
15110 Frederick Road
Woodbine, MD 21797

H. S. Matsuda, Manager
Composite Materials Laboratory
Pioneering R&D Laboratories
Toray Industries, Inc.
Sonoyama, Otsu, Shiga
JAPAN 520

J. R. McConnell
Tumac Industries, Inc.
650 Ford St.
Colorado Springs, CO 80915

James Meiggs
Kaman Sciences Corporation
P.O. Box 7463
Colorado Springs, CO 80933

R. N. Meroney
Colorado State University
Department of Civil Engineering
Fort Collins, CO 80521

G. N. Monsson
Department of Economic Planning
and Development
Barrett Building
Cheyenne, WY 82002

NASA Lewis Research Center (4)
21000 Brookpark Road
Cleveland, OH 44135
Attn: J. Savino
R. L. Thomas
W. Robbins
K. Kaza

Anthony A. Nedd
The Power Company, Inc.
P.O. Box 221
Genesee Depot, WI 53217

V. Nelson
West Texas State University
Department of Physics
P.O. Box 248
Canyon, TX 79016

Leander Nichols
Natural Power, Inc.
New Boston, NH 03070

Fred Nitzche
1 B Abrams
Escondido Village

Ronald Nousain
P.O. Box 111
Rome 1132
Los Angeles, CA 90051

Oklahoma State University (2)
Stillwater, OK 76074
Attn: W. L. Hughes
EE Department
D. K. McLaughlin
ME Department

Oregon State University (2)
Corvallis, OR 97331
Attn: R. E. Wilson
ME Department
R. W. Thresher
ME Department

Pat F. O'Rourke
Precinct 4
County Commissioner
City-County Building
El Paso, TX 79901

H. H. Paalman
Dow Chemical USA
Research Center
2800 Mitchell Drive
Walnut Creek, CA 94598

R. A. Parmelee
Northwestern University
Department of Civil Engineering
Evanston, IL 60201

Helge Petersen
Riso National Laboratory
DK-4000 Roskilde
DENMARK

Wilson Prichett, III
National Rural Electric
Cooperative Association
1800 Massachusetts Avenue NW
Washington, DC 20036

Dr. Barry Rawlings, Chief
Division of Mechanical Engineering
Commonwealth Scientific and
Research Organization Industrial
Graham Road, Highett
Victoria, 3190
AUSTRALIA

Thomas W. Reddoch
Associate Professor
Department of Electrical Engineering
The University of Tennessee
Knoxville, TN 37916

Ray G. Richards
Atlantic Wind Test Site
P.O. Box 189
Tignish P.E.I.
COB 2BO CANADA

A. Robb
Memorial University of
Newfoundland
Faculty of Engineering
and Applied Sciences
St. John's Newfoundland
CANADA A1C 5S7

Dr. -Ing. Hans Ruscheweyh
Institut fur Leichbau
Technische Hochschule Aachen
Wullnerstrasse 7
GERMANY

Gwen Schreiner
Librarian
National Atomic Museum
Albuquerque, NM 87185

Douglas B. Seely, P.E.
U.S. Department of Energy
P.O. Box 3621
102 NE Holladay
Portland, OR 97208

Arnan Seginer
Professor of Aerodynamics
Technion-Israel Institute of
Technology
Department of Aeronautical
Engineering
Haifa, ISRAEL

Dr. Horst Selzer
Dipl.-Phys.
Wehrtechnik und Energieforschung
ERNO-Raumfahrttechnik GmbH
Hunefeldstr. 1-5
Postfach 10 59 09
2800 Bremen 1
GERMANY

H. Sevier
Rocket and Space Division
Bristol Aerospace Ltd.
P.O. Box 874
Winnipeg, Manitoba
CANADA R3C 2S4

P. N. Shankar
Aerodynamics Division
National Aeronautical Laboratory
Bangalore 560017
INDIA

David Sharpe
Kingston Polytechnic
Canbury Park Road
Kingston, Surrey
UNITED KINGDOM

D. G. Shepherd
Cornell University
Sibley School of Mechanical and
Aerospace Engineering
Ithaca, NY 14853

Dr. Fred Smith
Mechanical Engineering Department
Head
Colorado State University
Ft. Collins, CO 80521

Kent Smith
Instituto Technologico Costa Rica
Apartado 159 Cartago
COSTA RICA

Leo H. Soderholm
Iowa State University
Agricultural Engineering, Room 213
Ames, IA 50010

Bent Sorenson
Roskilde University Centery
Energy JGroup, Bldg. 17.2
IMFUFA
P.O. Box 260
DK-400 Roskilde
DENMARK

Southwest Research Institute (2)
P.O. Drawer 28501
San Antonio, TX 78284
Attn: W. L. Donaldson,
R. K. Swanson

Rick Stevenson
Route 2
Box 85
Springfield, MO 65802

Dale T. Stjernholm, P.E.
Mechanical Design Engineer
Morey/Stjernholm and Associates
1050 Magnolia Street
Colorado Springs, CO 80907

G. W. Stricker
383 Van Gordon 30-559
Lakewood, CO 80228

C. J. Swet
Route 4
Box 358
Mt. Airy, MD 21771

John Taylor
National Research Council
ASEB
2101 Constitution Avenue
Washington, DC 20418

R. J. Templin (3)
Low Speed Aerodynamics Section
NRC-National Aeronautical
Establishment
Ottawa 7, Ontario
CANADA K1A OR6

Texas Tech University (3)
P.O. Box 4389
Lubbock, TX 79409
Attn: K. C. Mehta, CE Department
J. Strickland, ME Department
J. Lawrence, ME Department

Fred Thompson
Atari, Inc.
155 Moffett Park Drive
Sunnyvale, CA 94086

J. M. Turner, Group Leader
Terrestrial Energy Technology
Program Office
Energy Conversion Branch
Aerospace Power Division
Aero Propulsion Laboratory
Department of the Air Force
Air Force Wright Aeronautical
Laboratories (AFSC)
Wright-Patterson Air Force Base, OH
45433

United Engineers and
Constructors, Inc.
Advanced Engineering Department
30 South 17th Street
Philadelphia, PA 19101
Attn: A. J. Karalis

University of New Mexico (2)
New Mexico Engineering Research
Institute
Campus, P.O. Box 25
Albuquerque, N.M. 87131
Attn: G. G. Leigh

University of New Mexico (2)
Albuquerque, NM 87106
Attn: K. T. Feldman
Energy Research Center
V. Sloglund
ME Department

Jan Vacek
Eolienne experimentale
C.P. 279, Cap-aux-Meules
Iles de la Madeleine, Quebec
CANADA

Irwin E. Vas
Solar Energy Research Institute
1617 Cole Blvd.
Golden, CO 80401

Otto de Vries
National Aerospace Laboratory
Anthony Fokkerweg 2
Amsterdam 1017
THE NETHERLANDS

R. Walters
West Virginia University
Department of Aero Engineering
1062 Kountz Avenue
Morgantown, WV 26505

E. J. Warchol
Bonneville Power Administration
P.O. Box 3621
Portland, OR 97225

D. F. Warne, Manager
Energy and Power Systems
ERA Ltd.
Cleeve Rd.
Leatherhead
Surrey KT22 7SA
ENGLAND

G. R. Watson, Project Manager
The Energy Center
Pennine House
4 Osborne Terrace
Newcastle upon Tyne NE2 1NE
UNITED KINGDOM

R. J. Watson
Watson Bowman Associates, Inc.
1280 Niagara St.
Buffalo, NY 14213

R. G. Watts
Tulane University
Department of Mechanical Engineering
New Orleans, LA 70018

W. G. Wells, P.E.
Associate Professor
Mechanical Engineering Department
Mississippi State University
Mississippi State, MS 39762

T. Wentink, Jr.
University of Alaska
Geophysical Institute
Fairbanks, AK 99701

West Texas State University
Government Depository Library
Number 613
Canyon, TX 79015

Wind Energy Report
Box 14
102 S. Village Ave.
Rockville Centre, NY 11571
Attn: Farrell Smith Seiler

Wind Program Manager
Wisconsin Division of State Energy
8th Floor
101 South Webster Street
Madison, WI 53702

Richard E. Wong
Assistant Director
Central Solar Energy Research Corp.
1200 Sixth Street
328 Executive Plaza
Detroit, MI 48226

1000 G. A. Fowler
1200 L. D. Smith
3141 T. L. Werner (5)
3151 W. L. Garner (3)
For DOE/TIC (Unlimited Release)
3161 J. E. Mitchell (15)
3161 P. S. Wilson
4533 J. W. Reed
4700 J. H. Scott
4710 G. E. Brandvold
4715 R. H. Braasch (200)
4715 J. D. Cyrus
4715 R. D. Grover
4715 E. G. Kadlec
4715 P. C. Klimas
4715 M. T. Mattison
4715 R. O. Nellums
4715 W. N. Sullivan
4715 R. A. Watson
4715 D. F. Wolf
4715 M. H. Worstell
5500 O. E. Jones
5510 D. B. Hayes
5520 T. B. Lane
5523 R. C. Reuter, Jr.
5523 T. G. Carne
5523 D. B. Clauss (25)
5523 D. W. Lobitz
5523 D. A. Popelka
5523 P. S. Veers
5530 W. Herrmann
5600 D. B. Schuster
5620 M. M. Newsom
5630 R. C. Maydew
5633 R. E. Sheldahl
5636 J. K. Cole
5636 D. E. Berg
5636 W. H. Curry
8266 E. A. Aas
DOE/TIC (25)
(R. P. Campbell, 3172-3)

☆U.S. GOVERNMENT PRINTING OFFICE: 1981-0-777-023/558